Momentum and Energy Transfer in Wind Generation of Waves

CHIN-TSAU HSU

Fluid Mechanics Department, TRW Space and Technology Group, Redondo Beach, CA 90278

HONG-YE WU

Tetra Tech Incorporated, Pasadena, CA 91107

EN-YUN HSU AND ROBERT L. STREET

Department of Civil Engineering, Stanford University, Stanford, CA 94305

(Manuscript received 29 July 1981, in final form 27 May 1982)

ABSTRACT

Complete expressions for wind momentum and energy transfer to wind-generated waves are derived based on a boundary-layer integral method. The airflow and wave measurements as made by Wu *et al.* (1977, 1979) are used to provide a first-order estimate of the momentum and energy budget. The momentum and energy transfer to waves are found to be dominated by the wave-induced pressure and mainly received by the dominant wave, which agree with the wind energy input mechanism of a nonlinear wind-waves model proposed by Lake and Yuen (1978) and Yuen and Lake (1979). It is found that the waves support about 61% of the total wind momentum, but receive only about 29% of the total wind energy across the interface. This low fraction of energy to the waves is found to be the consequence of a high ratio of mean surface current velocity to wave celerity which results in a considerable leakage of energy delivered by the wave-supported momentum to the current. The measured energy transfer to waves by the wave-induced pressure is found to be in good agreement with that observed by others in the laboratory and in the field. The comparison of wave-growth parameter based on the wave-induced pressure to the field observations of Snyder *et al.* (1981) and to the predictions of Al-Zanaidi and Hui (1981) shows a strong dependence of the wave-growth parameter on the wave slope.

Based on the side-band instability theory of Benjamin and Feir (1967) and the nonlinear wave-modulation theory of Yuen and Lake (1980), the down-shifting of dominant wave frequency f_0 along the fetch x_1 is found to be described by $f_0 u_*/g = 0.91(x_1 g/u_*^2)^{-5/16}$, where u_* is the wind friction velocity and g the gravitational acceleration. As a result, the dominant wave slope $k_0\bar{a}$ changes with the fetch as $k_0\bar{a} = 0.58 \times (x_1 g/u_*^2)^{-1/8}$; this implies an evolution of the wind wave from a bounded, nonlinear system at short fetch to a free linear system at large fetch (a fully developed sea state). The decrease in the saturation range constant (Phillips, 1958, 1977) with increasing fetch is found to be closely related to this evolution.

1. Introduction

From Barnett (1968) and Hasselmann *et al.* (1973, 1976) it appears that the spectral evolution of ocean waves is primarily determined by energy sources associated with wind action, nonlinear wave-wave interaction and wave dissipation (mainly wave breaking). Because nonlinear wave-wave interaction describes only the redistribution of energy within the wave spectrum, its greatest importance lies in accomplishing the continuous shifting of the dominant wave frequency to lower frequency ranges. The wave dissipation represents the energy drain to current and oceanic turbulence from the waves. The energy input from the wind constitutes the most important facet in the energy budget of the coupled air-sea system during the growth period of surface waves.

The pioneering works by Phillips (1957) and Miles (1957) give two independent, but complementary mechanisms for generation of waves by the wind. While the resonance mechanism of Phillips gives a linear wave growth rate and is responsible for the initiation of waves,[1] Miles' mechanism produces an exponential growth rate and is more effective in transferring energy from wind to waves. However, the direct field measurements of Snyder and Cox (1966) and Barnett and Wilkerson (1967) and later the laboratory measurement of Bole and Hsu (1969) for a mechanically generated water wave showed that the wave growth rates were considerably greater than Miles' predictions. The discrepancy between the ob-

[1] Recently, Kawai (1979) found that the initiation of gravity-capillary waves is caused by the shear flow instability mechanism (Miles, 1962).

0022-3670/82/090929-23$09.75

servations and the predictions may be due to the following effects which were neglected in Miles' model: 1) the ocean waves are usually random and two-dimensional and 2) the wind is turbulent. The multiple components in the two-dimensional ocean wave field may lead to nonlinear wave-wave interaction (Hasselmann, 1962, 1963, 1966, 1967) with the result of a higher observed growth rate of the dominant waves. The interaction between the wave and the wind turbulence produces the wave-induced turbulent Reynolds stresses which may not only result in the direct energy transfer to wave, but may also stimulate energy transfer to the wave by the wave-induced pressure.

To evaluate the turbulent effect, theoretical closure models for the wave-induced turbulent Reynolds stresses have been used (Long, 1971; Saeger and Reynolds, 1971; Davis, 1970, 1972; Townsend, 1972; Gent and Taylor, 1976; Gent, 1977). Of particular interest are those of Gent and Taylor (1976) and Gent (1977) which studied the wave-induced flow under the conditions of finite amplitude waves and of distributed surface roughness along the wave profiles. Their general conclusion is that the amplitude and roughness effects are significant, although there is some inconsistency in their results. As the wind-generated waves are usually random, two-dimensional, composed of multiple components and sometimes of large amplitudes, where the short waves riding on the dominant wave are related to the surface roughness, the wave-induced flowfields as well as the momentum and energy transfer across the interface for a wind-generated water wave are expected to be different to some degree from those for wind over a smooth, mechanically-generated monochromatic wave.

The structure of the induced turbulent Reynolds stresses and the energy budget have been detailed by Hsu *et al.* (1981, 1982) for a mechanically-generated water wave. They observed that the relationships between the wave-induced velocities and the induced turbulent Reynolds stresses are basically of an eddy viscosity type. Their data also showed that the turbulence produces little direct energy transfer from wind to waves, but the transfer rate based on the measured wave-associated Reynolds stress is one order of magnitude greater than Miles' prediction.

In this paper, we extend our discussion of the momentum and energy budget to random and two-dimensional, wind-generated waves. The complete transfer expressions are first derived to indicate that the process responsible for the momentum and energy transfer across the interface are similar to those for winds over a mechanically-generated water wave obtained by Hsu *et al.* (1982), but with additional transfer due to the two-dimensionality of the waves. This similarity follows from the fact that the boundary-layer integral method employed in the analyses applies to an arbitrary form of the surface waves; however, the interpretations of the momentum and energy budget estimated based on the derived expressions may change with the characteristics of the surface waves.

It had been shown experimentally (Ramamonjiarisoa and Coantic, 1976; Lake and Yuen, 1978) that the wind-generated waves in a laboratory facility of short fetch are nonlinear, forced, bounded waves. According to the nonlinear wind wave model proposed by Lake and Yuen (1978) and Yuen and Lake (1979), the energy transfer from wind to waves is received mainly by the dominant waves. It follows from Deardorff (1967) that the wave-induced air pressure correlated with the dominant waves is the dominant force responsible for the energy transfer to the waves. This type of energy transfer mechanism differs significantly from that usually cited for the ocean waves where the measurements (Snyder *et al.*, 1981) indicated that the dominant waves receive only a small portion of the momentum and energy transfer from wind to waves, with a large portion received by the waves in the high-frequency range.

Although our analyses indicate that a complete, detailed estimate of the momentum and energy budget for the wind-generated waves requires simultaneous measurement of a two-dimensional wind wave spectrum, all three components of the air velocity, and air pressure, in a wave-following coordinate system, a first look at the budget is provided by using the simpler fixed frame measurement of two components of the air velocity and the air pressure, together with a single point measurement of the wave height, as carried out by Wu *et al.* (1977, 1979). The uncertainty associated with the simple experiment is sizable, estimated to be approximately 20%, but is not large enough to affect the main conclusions reached because 1) the additional transfer due to the two-dimensionality of the waves is practically negligible for the narrow directional wind wave spectrum, 2) the wave-induced pressure is found to be the dominant force in transferring the momentum and the energy to the waves, and 3) the air pressure measurement is not sensitive to whether a fixed or a wave-following frame are used (Snyder *et al.*, 1981).

The momentum and energy budgets estimated in this study are based on the nonlinear wind-wave model of Lake and Yuen (1978) and Yuen and Lake (1979) since the wavefield in the laboratory experiment of Wu *et al.* (1977, 1979) is essentially a nonlinear wind wave system. The results of our study confirm the wind energy input mechanism of the nonlinear wind wave model, i.e., that the wave-induced pressure is the dominant force for energy transfer from wind to waves. The development of the wind-generated waves along the fetch as described by the nonlinear wind wave model is discussed. The comparisons of the laboratory and the ocean data indicate that the nonlinearity of the wind wave system

decreases with increasing fetch. This implies that a nonlinear wind wave system at short fetch will evolve continuously into a linear free wave system at large fetch under the action of the wind. The decrease in the saturation range constant (Phillips, 1977, p. 147) with increasing fetch is found to be closely related to this evolution from nonlinear to linear wind wave systems. The nonlinear wave-wave interaction mechanism for a linear free wave system (Hasselmann, 1962, 1963, 1966 and 1967) is not expected to have a significant role in a laboratory facility of short fetch, although its role may become substantial in the ocean where the fetch is large.

2. Definition and description of the flowfields

Considering a turbulent wind blowing over a water surface which is originally calm, we assume that the wind duration is long enough so that the processes that govern the generation of waves at the interface of the coupled air-water system are statistically stationary. The fetch for the development of the wind-generated waves is also assumed large enough so that the wave spectrum is dominated by gravity waves. The right-handed coordinate system x_i is arranged such that x_1 is in the mean wind direction, x_2 in the horizontal direction normal to the wind and x_3 in the vertical direction measured upward from the mean water level. The surface displacement $\tilde{\eta}$, which describes the wind-generated wave field, is a random function of x_1, x_2 and t and has a symmetrical spectrum with respect to the x_1 axis. The wind wave spectrum is assumed to grow weakly in the x_1 direction and to be homogeneous in x_2. Accordingly, the statistical expectation of flow quantities is independent of x_2 and time t; however, it may be weakly dependent on x_1 and strongly dependent on x_3 according to boundary layer theory.

With the existence of the surface wave field, the wind velocity, pressure, and turbulent Reynolds stresses are expressed as

$$\left.\begin{aligned} u_i &= \bar{u}_i + \tilde{u}_i + u_i' \\ p &= \bar{p} + \tilde{p} + p' \\ u_i'u_j' = r_{ij} &= \bar{r}_{ij} + \tilde{r}_{ij} + r_{ij}' \end{aligned}\right\}, \quad (2.1a,b,c)$$

where $\bar{u}_i$, $\bar{p}$ and $\bar{r}_{ij}$ are mean flow quantities, $\tilde{u}_i$, $\tilde{p}$ and $\tilde{r}_{ij}$ are perturbations induced by the surface waves, and u_i', p' and r_{ij}' are turbulent fluctuations. The wave-induced quantities are random but are coherent with $\tilde{\eta}$. Because both the wave-induced component and the turbulent component are random, they cannot be decomposed directly. However, the statistical behaviors of the wave-induced flow can be extracted by correlating u_i, p and r_{ij} to the surface wavefield.

For a stationary process, a mean flow quantity $\bar{u}_i$ can be obtained by taking a time average of a total flow quantity u_i. However, as shown by Hsu *et al.* (1981, 1982), a time average performed at a fixed position produces ambiguities in representing flowfields near the interface because no time-averaged result can be obtained for $x_3 < |\tilde{\eta}|_{\max}$. An extrapolation from $x_3 = h + \tilde{\eta}$ to $x_3 = h$ by using a Taylor series expansion usually leaves us with difficulty in interpreting the actual physical meaning of the wave-induced flow. To circumvent these difficulties, a transformed wave-following frame was used. In the wave-following frame, the time average is performed at fixed x_1 and x_2 but at a time varying position x_3 given by

$$x_3 = x_3^* + f(x_3^*)\tilde{\eta}, \quad (2.2)$$

where $f(x_3^*)$ satisfies $f(0) = 1$ and decays monotonically to zero for large x_3^* (far away from the interface). The representation of the air flowfields in the wave-following frame is complete for all $x_3^* \geq 0$ and the difference between flow quantities measured in the fixed and the wave-following frames can be established. However, if a flow quantity is integrated vertically upward from the interface, the resultant integral is a function of x_1, x_2 and t and can be time averaged in the usual way. The details of $f(x_3^*)$ in $0 < x_3^* < \infty$ are not critical to the results of the integral analysis.

For a wind-generated wave system the fluctuations around the mean quantity contain both the wave-induced and the turbulent components and these can not be separated experimentally. Therefore, the physical (or mathematical) meaning of the wave-induced quantity remains to be defined. From the existing turbulence theory and the relationship between the wave-induced quantity and the wave, we shall define the wave-induced quantity $\tilde{g}$ in $\tilde{g} + g'$ as the component whose coherence to the wave $\tilde{\eta}$ is equal to unity. Hence, a fluctuation whose coherence to $\tilde{\eta}$ is less than 1 contains turbulent components and a fluctuation with zero coherence to $\tilde{\eta}$ is a purely turbulent quantity.

For the convenience of discussing the turbulent effect, (2.1a,b,c) is rewritten as

$$\left.\begin{aligned} u_i &= \langle u_i \rangle + u_i' \\ p &= \langle p \rangle + p' \\ u_i'u_j' &= \langle r_{ij} \rangle + r_{ij}' \end{aligned}\right\}, \quad (2.3a,b,c)$$

where $\langle u_i \rangle = \bar{u}_i + \tilde{u}_i$, $\langle p \rangle = \bar{p} + \tilde{p}$ and $\langle r_{ij} \rangle = \bar{r}_{ij} + \tilde{r}_{ij}$ are the components excluding turbulent fluctuations. No specific definition for the angle braces is made here for the wind-generated waves since $\tilde{\eta}$ represents both the dominant wave and the ripples whose phase relationships are not fixed; however, these braces become the phase averages if $\tilde{\eta}$ represents the mechanically-generated wave studied by Hsu *et al.* (1981, 1982). For this study, we shall assume that

the air turbulence is suppressed at the interface so that the velocity fluctuations at the interface are entirely related to the surface wave motion, since the density difference between the air and the water is very large. Hence, we have $u_i' = 0$, $u_i = \langle u_i \rangle = (\bar{u}_0 + \tilde{u}_1, \tilde{u}_2, \tilde{u}_3)$ and $u_i'u_j' = \langle r_{ij} \rangle = 0$ at $x_3 = \tilde{\eta}$, where $\bar{u}_0$ is the mean surface drift current velocity. We shall also assume that no large-scale wave breaking occurs to entrain air into the water. The condition of no air flow across the interface requires that

$$\tilde{u}_3 = \langle u_3 \rangle = \frac{\partial \tilde{\eta}}{\partial t} + \langle u_k \rangle \frac{\partial \tilde{\eta}}{\partial x_k} \quad (k = 1, 2) \quad (2.4)$$

as the interface boundary condition for $\tilde{u}_3$. Hereafter, we adopt the convention that a repeated English letter index denotes a summation over the index. The summation runs from 1 to 3 for i and j and from 1 to 2 for k. A Greek letter is then used to denote an index over which no summation occurs even when the index is repeated.

3. Momentum transfer across the interface

We suppose that a boundary layer forms in the air flow over the interface and develops appropriate integral relations. The equations describing the conservation of mass and momentum for an incompressible flow are

$$\frac{\partial u_i}{\partial x_i} = 0, \quad (3.1)$$

$$\rho \frac{\partial u_i}{\partial t} + \rho \frac{\partial}{\partial x_j}(u_i u_j) = -\frac{\partial p}{\partial x_j}\delta_{ij} + \frac{\partial}{\partial x_j}\tau_{ij}, \quad (3.2)$$

where δ_{ij} is the Kronecker delta, ρ is the air density,

$$\tau_{ij} = \rho\nu\left(\frac{\partial u_i}{\partial x_j} + \frac{\partial u_j}{\partial x_i}\right)$$

is the viscous stress and ν the kinematic viscosity. In the free stream, where the flow is steady and potential and the viscous effect is negligible, (3.2) reduces to

$$\rho U_\infty \frac{\partial U_\infty}{\partial x_1}\delta_{1i} = -\frac{\partial P_\infty}{\partial x_1}\delta_{1i}, \quad (3.3)$$

where U_∞ and P_∞ are the values of $\bar{u}_1$ and $\bar{p}$ in the free stream, respectively. Subtracting (3.2) from (3.3), applying the continuity equation (3.1) and substituting (2.3a,b,c) into the resultant equation yields

$$\rho \frac{\partial}{\partial t}(U_\infty\delta_{1i} - \langle u_i \rangle) + \rho \frac{\partial}{\partial x_j}[\langle u_j \rangle (U_\infty\delta_{1i} - \langle u_i \rangle)] + \rho(U_\infty - \langle u_1 \rangle)\frac{\partial U_\infty}{\partial x_1}\delta_{1i} + \frac{\partial}{\partial x_j}\sigma_{ij} + T_i' = 0, \quad (3.4)$$

where

$$\sigma_{ij} = (P_\infty - \langle p \rangle)\delta_{ij} - \rho\langle r_{ij} \rangle + \langle \tau_{ij} \rangle \quad (3.5)$$

and T_i' denotes the sum of turbulent fluctuating terms which are not coherent with the surface waves. The stress σ_{ij}, which is defined relative to the pressure stress in the free stream, acts in the i-direction and on the plane normal to the j-axis.

If we integrate (3.4) with respect to x_3 from $\tilde{\eta}$ to ∞ (the free stream), apply the identities

$$\int_{\tilde{\eta}}^{\infty} \frac{\partial g_i}{\partial t}\,dx_3 = \frac{\partial}{\partial t}\left[\int_{\tilde{\eta}}^{\infty} g_i dx_3\right] + \left(g_i \frac{\partial \tilde{\eta}}{\partial t}\right)_0, \quad (3.6)$$

$$\int_{\tilde{\eta}}^{\infty} \frac{\partial g_{ij}}{\partial x_j}\,dx_3 = \frac{\partial}{\partial x_k}\left[\int_{\tilde{\eta}}^{\infty} g_{ik}dx_3\right] + \left(g_{ik}\frac{\partial \tilde{\eta}}{\partial x_k}\right)_0 + (g_{i3})_\infty - (g_{i3})_0 \quad (3.7)$$

(where the subscripts 0 and ∞ denote the quantities evaluated at the interface $x_3 = \tilde{\eta}(x_3^* = 0)$ and at the free stream, respectively), invoke the interface boundary condition (2.4), and take time averages, we have

$$\rho \frac{\partial}{\partial t}(U_\infty\theta_i) + \rho \frac{\partial}{\partial x_k}(U_\infty{}^2\theta_{ik}) - \rho W_\infty{}^2\delta_{3i} + \rho U_\infty \frac{\partial U_\infty}{\partial x_1}\theta_1\delta_{1i} + \frac{\partial}{\partial x_k}\overline{\left[\int_{\tilde{\eta}}^{\infty} \sigma_{ik}dx_3\right]} = \overline{(\sigma_{i3})_0} - \overline{(\sigma_{ik})_0 \frac{\partial \tilde{\eta}}{\partial x_k}}. \quad (3.8)$$

In (3.8),

$$\theta_i = \overline{\int_{\tilde{\eta}}^{\infty}\left(\delta_{1i} - \frac{\langle u_i \rangle}{U_\infty}\right)dx_3}$$

is the displacement thickness of the i-component velocity,

$$\theta_{ik} = \overline{\int_{\tilde{\eta}}^{\infty}\frac{\langle u_k \rangle}{U_\infty}\left(\delta_{1i} - \frac{\langle u_i \rangle}{U_\infty}\right)dx_3}$$

is the momentum thickness tensor resulting from the convection of the i-component velocity deficit by the k-component velocity, and

$$W_\infty = (\bar{u}_3)_\infty = -\frac{\partial}{\partial x_1}\overline{\left[\int_{\tilde{\eta}}^{\infty}\langle u_1 \rangle dx_3\right]}$$

is the fluid entrainment rate from the free stream to the developing boundary layer. The terms on the left-hand side of (3.8) represent the momentum loss from the air flow in the boundary layer; this momentum loss is expressed as the momentum transfer across the interface, as indicated by the terms appearing on the right-hand side of (3.8).

On the right-hand side of (3.8) the first term is the mean stress acting on the plane of the mean water surface and is not related to the surface waves. Hence, it represents the mean momentum transferred to the drift current, i.e.,

$$\bar{M}_{ci} = \overline{(\sigma_{i3})_0} = (P_\infty - \bar{p}_0)\delta_{i3} - \overline{\rho\langle r_{i3}\rangle_0} + \overline{\langle \tau_{i3}\rangle_0} . \quad (3.9)$$

The second term (with $\partial\tilde{\eta}/\partial x_k$) describes the mean momentum flux supported by the surface waves. It appears as a form drag. The negative sign implies that a higher pressure on the windward and lower pressure on the leeward of the waves will produce a positive momentum transfer from wind to waves. Consequently, the momentum transfer to the waves is given by

$$\bar{M}_{wi} = \overline{-(\sigma_{ik})_0 \frac{\partial\tilde{\eta}}{\partial x_k}} = \overline{(\tilde{p}\delta_{ik} + \rho\tilde{r}_{ik} - \tilde{\tau}_{ik})_0 \frac{\partial\tilde{\eta}}{\partial x_k}} \quad (3.10)$$

and the total mean momentum transferred across the interface is

$$\bar{M}_i = \bar{M}_{ci} + \bar{M}_{wi} .$$

Upward momentum flux is positive according to our coordinate system. We want to emphasize that the wave-induced quantities in (3.10) are those observed in the wave-following frame as defined by (2.2), because these quantities were evaluated at $x_3 = \tilde{\eta}$ before the time averages were taken.

Using the argument made by Hsu *et al.* (1982), it can be shown that $\bar{M}_{c3} = 0$ so that distribution of P_∞ along x_1 only represents the slight tilting of the mean water surface. Thus, assuming a horizontal mean water surface does not produce a significant effect on the analysis. To the first approximation, it can be shown that $\bar{M}_{w3} = -\overline{\rho(\tilde{u}_3\tilde{u}_3)_0}$; the vertical momentum supported by the wave is the one resulting from the vertical wave oscillation and has little consequence to the wave's growth. Because at the interface $\bar{r}_{23} = \bar{\tau}_{23} = 0$ due to $\bar{u}_2 = 0$, we find $\bar{M}_{c2} = 0$; the symmetry in the wind wave spectrum with respect to x_1-axis also suggests that $\bar{M}_{w2} = 0$. This leaves $\bar{M}_1$ as the only transfer of interest. Comparing (3.9) and (3.10) for $i = 1$ to the equivalent expressions obtained by Hsu *et al.* (1982) for flows over a mechanically-generated water wave, we find that, while the expressions for the transfer to the current are identical, the expressions for the transfer to the waves are different because there are additional terms

$$\overline{(\rho\tilde{r}_{12} - \tilde{\tau}_{12})_0 \frac{\partial\tilde{\eta}}{\partial x_2}}$$

appearing in (3.10). This difference is due to the two-dimensionality of the wind wave spectrum.

If (3.2) is evaluated at $x_3 = \tilde{\eta}$ for $i = 1$ and correlated with $\tilde{\eta}$, following the procedures used by Hsu *et al.* (1982), neglecting the triple correlation and recalling that $\partial/\partial x_2$ of a mean quantity is zero, we find

$$\bar{M}_{w1} = -\overline{\rho(\tilde{u}_1\tilde{u}_3)_0} + \overline{\tilde{\eta}\frac{\partial}{\partial x_3}(\rho\tilde{r}_{13} - \tilde{\tau}_{13})_0} + \frac{\partial}{\partial x_1}\overline{[(\tilde{p} + \rho\tilde{r}_{11} - \tilde{\tau}_{13})\tilde{\eta}]_0} + \frac{\partial}{\partial x_1}\overline{(\rho\tilde{u}_0\tilde{u}_1\tilde{\eta})_0} . \quad (3.11)$$

In (3.11) the dependence of mean quantities on x_1 results from the developing wind waves and boundary layer. When the development of wind waves and boundary layer is so weak that the x_1-dependent terms in (3.11) are insignificant, we have

$$\bar{M}_{w1} = -\overline{\rho(\tilde{u}_1\tilde{u}_3)_0} + \overline{\tilde{\eta}\frac{\partial}{\partial x_3}(\rho\tilde{r}_{13} - \tilde{\tau}_{13})_0} . \quad (3.12)$$

To provide an insight to (3.12), we first perform a time average on (2.4) and find $\overline{\tilde{u}_k\partial\tilde{\eta}/\partial x_k} = 0$, i.e., $\tilde{u}_k$ are in quadrature with $\partial\tilde{\eta}/\partial x_k$. This would imply that $\tilde{u}_k$ are also in quadrature with $\partial\tilde{\eta}/\partial t$ since the wave frequency and the wavenumber are interdependent [see Eq. (6.9)]. If (2.4) is multiplied by $\tilde{u}_1$ and the time average is taken, we find, to the second order of wave slope, $\overline{(\tilde{u}_1\tilde{u}_3)_0} = 0$. Hence, we conclude that the shear stress gradient at the interface is significant in order to produce a momentum transfer $\bar{M}_{w1}$ at the second order of wave slope. This large shear stress gradient is expected to hold only in the viscous sublayer at the interface. The viscous sublayer is a very thin layer as compared to the mean wave amplitude and is undulated with the surface wave. Outside the viscous sublayer, however, the viscous stresses are presumably negligible and $\overline{(\tilde{u}_1\tilde{u}_3)_{\delta_0}}$ is usually non-zero and large; here the subscript δ_0 means that the term is evaluated at $x_3 = \tilde{\eta} + \delta_0$ with δ_0 being the mean thickness of the viscous sublayer. Eqs. (3.9), (3.10) and (3.12) then reduce to

$$\bar{M}_{c1} = -\rho(\bar{r}_{13})_{\delta_0} , \quad (3.13)$$

$$\bar{M}_{w1} = \overline{\left(\tilde{p}\frac{\partial\tilde{\eta}}{\partial x_1}\right)_{\delta_0}} + \rho\overline{\left(\tilde{r}_{11}\frac{\partial\tilde{\eta}}{\partial x_1} + \tilde{r}_{12}\frac{\partial\tilde{\eta}}{\partial x_2}\right)_{\delta_0}} , \quad (3.14)$$

$$= -\overline{\rho(\tilde{u}_1\tilde{u}_3)_{\delta_0}} + \rho\overline{\tilde{\eta}\left(\frac{\partial}{\partial x_3}\tilde{r}_{13}\right)_{\delta_0}} . \quad (3.15)$$

The ratio of momentum flux supported by the waves to the total momentum flux across the interface is then given by

$$\gamma_M = \bar{M}_{w1}/\bar{M}_1 . \quad (3.16)$$

4. Energy transfer across the interface

We now consider the energy transfer across the interface and determine the portion of energy transfer which is available for growth of the wind-generated

waves. To begin, we refer back to (3.4). If (3.4) is evaluated for a particular component ($i = \alpha$) and multiplied by $\langle u_\alpha \rangle$, a few manipulations and application of the continuity equation produce

$$\frac{\rho}{2}\frac{\partial}{\partial t}[\langle u_\alpha\rangle(U_\infty\delta_{1\alpha} - \langle u_\alpha\rangle)] + \frac{\rho}{2}U_\infty{}^2\frac{\partial}{\partial t}\left(\delta_{1\alpha} - \frac{\langle u_\alpha\rangle}{U_\infty}\right)\delta_{1\alpha} + \frac{\rho}{2}\frac{\partial}{\partial x_j} \times [\langle u_j\rangle(U_\infty{}^2\delta_{1\alpha}\delta_{1\alpha} - \langle u_\alpha\rangle\langle u_\alpha\rangle)] - \frac{\partial}{\partial x_j}[\langle u_\alpha\rangle\sigma_{\alpha j}] + \sigma_{\alpha j}\frac{\partial\langle u_\alpha\rangle}{\partial x_j} + T'_{\alpha\alpha} = 0, \quad (4.1)$$

where $T'_{\alpha\alpha}$ is the turbulent fluctuating term which is not coherent with the wave field. Integrating (4.1) with respect to x_3 from $\tilde{\eta}$ to ∞, invoking (3.6) and (3.7), applying the interface boundary condition (2.4) and taking the time averages yields

$$\frac{\rho}{2}\frac{\partial}{\partial t}(U_\infty{}^2\theta_{\alpha\alpha}) + \frac{\rho}{2}U_\infty{}^2\frac{\partial}{\partial t}(\theta_\alpha\delta_{1\alpha}) + \frac{\rho}{2}\frac{\partial}{\partial x_k}(U_\infty{}^3\theta_{\alpha\alpha k}) - \rho W_\infty{}^3\delta_{3\alpha} - \frac{\partial}{\partial x_k}\overline{\int_{\tilde{\eta}}^{\infty}\sigma_{\alpha k}\cdot\langle u_\alpha\rangle dx_3} + \overline{\int_{\tilde{\eta}}^{\infty}\sigma_{\alpha k}\cdot\frac{\partial\langle u_\alpha\rangle}{\partial x_k}dx_3} = \overline{(M_\alpha\langle u_\alpha\rangle)_0}, \quad (4.2)$$

where

$$\theta_{\alpha\alpha k} = \overline{\int_{\tilde{\eta}}^{\infty}\frac{\langle u_k\rangle}{U_\infty}\left(\delta_{1\alpha} - \frac{\langle u_\alpha\rangle^2}{U_\infty{}^2}\right)dx_3}$$

is the energy thickness tensor resulting from the convection of the α-component kinetic energy deficit by the k-component velocity.

On the left of (4.2), the first three terms represent the energy loss from the velocity field in the boundary layer; the fourth term is the supply of vertical kinetic energy due to fluid entrainment; the fifth term is the energy transport in the boundary layer by $\sigma_{\alpha k}$; and the sixth term is the energy drain to the external field in the boundary layer due to the stresses $\sigma_{\alpha k}$ working against the strain $\partial\langle u_\alpha\rangle/\partial x_k$. The energy drain by $\sigma_{\alpha k}$ includes the energy conversion from the α-component to other components of the kinetic energy caused by pressure straining, the energy drain to background turbulence caused by the turbulent Reynolds stresses $\langle r_{\alpha k}\rangle$, and the dissipation to internal thermal energy caused by the viscous stresses $\langle \tau_{\alpha k}\rangle$. The net energy loss above the interface as indicated by the left of (4.2) appears then as the energy flux $\bar{E}_{\alpha\alpha}$ transferred across the interface and given by the right of (4.2), namely,

$$\bar{E}_{\alpha\alpha} = \overline{(M_\alpha\langle u_\alpha\rangle)_0}.$$

Accordingly, the total energy transfer across the interface is $\bar{E}_{ii}$. If we decompose M_i into $\bar{M}_i + \tilde{M}_i$ and $\langle u_i\rangle$ into $\bar{u}_i + \tilde{u}_i$, we find

$$\bar{E}_{ii} = \bar{E}_c + \bar{E}_w,$$

where

$$\bar{E}_c = \bar{M}_i(\bar{u}_i)_0 = \bar{M}_1\bar{u}_0 \quad (4.3)$$

is the energy transfer to the drift current and

$$\bar{E}_w = \overline{(\tilde{M}_i\tilde{u}_i)_0} = \overline{(\tilde{\sigma}_{i3}\tilde{u}_i)_0} - \overline{\left(\sigma_{ik}\frac{\partial\tilde{\eta}}{\partial x_k}\tilde{u}_i\right)_0} \quad (4.4)$$

is the energy transfer to waves. Because $\tilde{u}_k$ and $\partial\tilde{\eta}/\partial x_k$ are in quadrature and $\bar{\sigma}_{12} = \bar{\sigma}_{21} = \bar{\sigma}_{32} = 0$, the term

$$\overline{\left(\sigma_{ik}\frac{\partial\tilde{\eta}}{\partial x_k}\tilde{u}_i\right)_0}$$

to the second order in wave slope of the dominant wave reduces to

$$(\bar{\sigma}_{31})_0\overline{\left(\frac{\partial\tilde{\eta}}{\partial x_1}\tilde{u}_3\right)_0}.$$

If the viscous terms in σ_{ik} are discarded outside the viscous sublayer, the energy transfer from wind to waves can be expressed as

$$\bar{E}_w = -\overline{(\tilde{p}\tilde{u}_3)_0} - \overline{\rho(\tilde{r}_{i3})_{\delta_0}(\tilde{u}_i)_0} + \rho(\bar{r}_{31})_{\delta_0}\overline{\left(\frac{\partial\tilde{\eta}}{\partial x_1}\tilde{u}_3\right)_0}. \quad (4.5)$$

The ratio of energy flux to waves to the total energy flux across the interface is

$$\gamma_E = \bar{E}_w/\bar{E}_{ii}. \quad (4.6)$$

5. Experiment

From the derivations given in Sections 3 and 4, it is clear that a correct and complete evaluation of the momentum and energy transfer processes can only be made by a simultaneous measurement of all three components of the air velocity, air pressure, and a two-dimensional surface wave spectrum in a wave-following coordinate system. While the results of such a measurement are not now available, a simpler measurement in the air of the horizontal and vertical velocity components and the pressure in a fixed frame, together with a single point measurement of the wave height, may provide reasonable estimates of the momentum and energy budgets of the windwave system. This simpler measurement was carried out by Wu *et al.* (1977, 1979). Before we present the momentum and energy budgets calculated from the data of Wu *et al.*, we shall review briefly the experimental conditions and discuss some potential limitations of the experiment.

a. Data acquisition

The experiment was conducted in the Stanford Wind, Water Wave Research Facility. A description of the facility can be found in the reports by Hsu (1965) and subsequent investigators. The setup of this experiment was described in detail by Wu *et al.* (1977, 1979). In summary, the wind field and the wave field were measured simultaneously by fixed probes at different fetches (x_1 = 3.46, 6.51, 9.48, 12.61 and 15.66 m) under stationary wind and wave conditions. At each station the data consist of mean velocity, pressure fluctuation, fluctuating velocities and wave height. The mean velocity was measured by a Pitot-static tube probe at different elevations to provide a velocity profile; the pressure and the fluctuating velocities were measured by a pressure sensor which consists of a pressure-sensing head and a crystal transducer and by an ×-array hot-film probe, respectively, at an elevation ~5 mm above the highest wave crest; the wave height was measured by a capacitance wave height gage. Three runs were made corresponding to mean free stream velocities of 7.26, 8.10 and 8.97 m s^{-1} at x_1 = 15.66 m. In this experiment, the boundary layer thickness over the water and on the side and top walls is less than 0.25 m (see Fig. 1); hence, for the channel with air height and width of 1 m, the effects of the channel roof and the side wall are negligible since the sensors are located at the middle of the channel.

The specifications of the pressure sensing head and the crystal transducer and the frequency calibrations of amplitude response and phase shift of the pressure sensor, as well as the specification and the calibration of the wave gage, were described by Wu *et al.* (1977, 1979); hence they are not elaborated here. Here we describe only the velocity probes. The Pitot-static tube probe is 0.038 cm in outer diameter. Two leads of total and static pressure were connected to a Pace differential pressure transducer (Model P90D) which was connected to a Sanborn 656-1100 carrier amplifier. The Pace transducer was calibrated against a Combust micromanometer which has a resolution of ±0.05 mm of water (equal to 0.49 Pa). The estimated uncertainty in the Pitot-static tube measurement is 3%.

The selected ×-array hot-film probe was a TSI Model 1240-20 on which the films were 1.016 mm long and 50.8 μm in diameter. The frequency response of the hot-films was up to 40 000 Hz as specified by the manufacturer. Each hot-film was driven by a TSI Model 1010A constant temperature anemometer. The hot-film probe and anemometer systems were calibrated against the Pitot-static tube *in situ* immediately before data taking. The uncertainty in the hot-film probe calibration was mainly caused by the uncertainty in the Pitot-static tube calibration and, hence, was approximately 3% for the mean velocity. However, for the measured turbulent quantities such as turbulent Reynolds stresses the uncertainty is higher and was estimated to be approximately 10%.

Except for the Pitot-static tube data, which were taken every 0.01 s for 2 min, all other data were taken every 0.025 s for 10.7 min. All the signals were approximately amplified and low-pass filtered at 20 Hz before data sampling. The sampling rate of 40 samples per second is adequate to provide good frequency resolution for the wave-induced flow (which has a frequency bandwidth less than 20 Hz), but not for the turbulence. In order to reveal the full frequency range of the turbulence characteristics, one extra set of velocity fluctuation data was taken at 5000 samples per second for 4 min and low-pass filtered at a 2500 Hz cutoff frequency. The data sampling and the data reduction (described in Section 6) were performed by an HP 2100A data acquisition-reduction system (Takeuchi and Mogel, 1975).

For details on the sensor calibrations and the procedures of data taking, the readers are referred to the original report by Wu *et al.* (1977).

b. Limitations in the experiment

In addition to the limitations and the uncertainties associated with the instrumentation described above, the use of the experimental results to estimate the momentum and energy budgets based on Eqs. (3.13)–(3.15) and (4.3) and (4.5) is still limited because the wind-generated waves are two-dimensional and because the measurement is not in the wave-following frame. However, under some circumstances the effects of two-dimensionality of the wind waves and of the fixed frame measurement may become insignificant if the dominant transfer mechanisms are not sensitive to the above effects.

According to Hasselmann (1963), the wind-wave spectrum $F(f, \theta)$ is assumed to be separable according to

$$F(f, \theta) = E(f) \cdot D'(\theta), \tag{5.1}$$

where $D'(\theta)$ is the spreading function. For field prediction, Barnett (1968) assumed

$$D'(\theta) = \begin{cases} \dfrac{8}{3\pi} \cos^4\theta, & \text{if } |\theta| \leqslant \pi/2 \\ 0, & \text{if } \pi/2 < |\theta| < \pi \end{cases} \tag{5.2}$$

if the wind is aligned with the dominant waves. The directional wave spectrum in a laboratory was measured by Rikiishi (1978); the cosine power in the spreading function was found to range from 3 to 6.5. This wide range in the cosine power was also observed in an earlier field experiment (Mitsuyasu *et al.*, 1975). However, the form (5.2) was used by Mitsuyasu and Rikiishi (1978) for wind-generated waves in a laboratory tank. In this study, we shall also use (5.2) to

provide a first-order correction for the effect of wave directionality (the use of a form with different cosine power will not alter our overall conclusions of this study).

With this presumed spreading function, the momentum transfer $\overline{\rho\tilde{r}_{12}\partial\tilde{\eta}/\partial x_2}$ caused by the two-dimensionality of the waves is small compared to the transfer $\overline{\rho\tilde{r}_{11}\partial\tilde{\eta}/\partial x_1}$ because the spreading factor

$$\int_{-\pi/2}^{\pi/2} D(\theta)\sin^2\theta d\theta \quad \text{for} \quad \overline{\rho\tilde{r}_{12}\partial\tilde{\eta}/\partial x_2}$$

is relatively small compared to the spreading factor

$$\int_{-\pi/2}^{\pi/2} D(\theta)\cos^2\theta d\theta \quad \text{for} \quad \overline{\rho\tilde{r}_{11}\partial\tilde{\eta}/\partial x_1}\,,$$

and also because the amplitude of $\tilde{r}_{12}$ is less than half of $\tilde{r}_{11}$ [see Hsu *et al.* (1981)]. Similar arguments can be applied also to the energy transfer by $\rho\tilde{r}_{23}$ due to the two-dimensionality of the surface waves. That the transfer due to two-dimensional waves is negligible becomes more obvious if the transfer is dominated by pressure; this, as we will see, is indeed the case. It follows also that replacing a three-dimensional velocity measurement by a two-dimensional one is justified. The assumed expressions (5.1) and (5.2) also allow us to replace the two-dimensional surface wave measurement by a single point measurement.

To delineate the difference due to the fixed-frame measurement, we shall start with the examination of the relationships that relate a fixed-frame quantity to a wave-following frame quantity. From Taylor series expansion the following relations to the second order in wave slope can be obtained:

$$\overline{\tilde{u}_1\tilde{u}_3(x_3)|_{x_3=0}} = \overline{\tilde{u}_1\tilde{u}_3(x_3^*)|_{x_3^*=0}}\,, \tag{5.3}$$

$$(-\rho\bar{r}_{13}+\bar{\tau}_{13})|_{x_3=0} = (-\rho\bar{r}_{13}+\bar{\tau}_{13})|_{x_3^*=0} + \overline{\tilde{\eta}\frac{\partial}{\partial x_3}(\rho\tilde{r}_{13}-\tilde{\tau}_{13})|_{x_3^*=0}}\,. \tag{5.4}$$

Note that the sum of the last terms of (5.3) and (5.4) is the total wave-supported momentum $\bar{M}_{w1}$ [see Eq. (3.12)]. The first term on the right-hand side of (5.4) is the total current-supported momentum $\bar{M}_{c1}$. Because (5.3) is equal to zero from the interface boundary condition, the last term on the right-hand side of (5.4) actually is the total momentum supported by the waves. Hence $(-\rho\bar{r}_{13}+\bar{\tau}_{13})_{x_3=0}$ actually includes the transfer to both current and waves and is the total momentum flux across the interface. Across the thin viscous sublayer, $\bar{M}_{c1}$ and $\bar{M}_{w1}$ remain constant and the viscous terms in (5.4) are negligible. However, $\overline{(\tilde{u}_1\tilde{u}_3)_{\delta_0}}$ becomes non-zero and

$$\overline{(\tilde{u}_1\tilde{u}_3)_{\delta_0}} \gg \overline{\tilde{\eta}\frac{\partial}{\partial x_3}\tilde{r}_{13}|_{\delta_0}}\,.$$

This implies that $(-\rho\bar{r}_{13}+\bar{\tau}_{13})_{x_3=h}$ is not constant in the viscous sublayer. The measurement of Hsu *et al.* (1982) indicates that $(\overline{\tilde{\eta}\partial\tilde{r}_{13}/\partial x_3})_{\delta_0}$ is also negligible as compared to $\bar{r}_{13}|_{\delta_0}$. This leads to

$$\bar{M}_{c1} = -\rho\bar{r}_{13}(x_3^*)|_{x_3^*=\delta_0} \approx -\rho\bar{r}_{13}(x_3)|_{x_3=\delta_0}\,,$$

$$\bar{M}_{w1} \approx \overline{\tilde{u}_1\tilde{u}_3(x_3^*)|_{x_3^*=\delta_0}} = \overline{\tilde{u}_1\tilde{u}_3(x_3)|_{x_3=\delta_0}}\,.$$

In this experiment the hot-film sensor is located in the logarithmic region of the mean velocity profile. In the logarithmic region, the turbulent Reynolds stress $-\rho\bar{r}_{13}$ remains constant and equal to $-\rho\bar{r}_{13}|_{\delta_0}$ as confirmed by the experiment of Hsu *et al.* (1981). Consequently, we expect that the measurement of $-\rho\bar{r}_{13}$ as made in this experiment gives a reasonable estimate of $\bar{M}_{c1}$.

On the other hand, according to the measurement of Hsu *et al.* (1981) we do not expect the value of $\overline{\tilde{u}_1\tilde{u}_3}(x_3)$ to be constant in the logarithmic region. The wave-induced fluctuations do not have the typical characteristics of mixing, vortex stretching and energy production, cascade and dissipation as those of turbulence. While the mean turbulent Reynolds stress $-\bar{r}_{13}$ is believed to be mainly produced by a bursting process, the wave-associated Reynolds stress $-\overline{\tilde{u}_1\tilde{u}_3}$ is produced by a critical layer mechanism. The critical layer is highly nonlinear and turbulently diffusive (Benney and Bergeron, 1969; Robinson, 1974; Hsu and Hsu, 1982). The nonlinear critical layer is considerably thicker than the viscous sublayer and extends deeply into the logarithmic region. The turbulence affects the production of $-\overline{\tilde{u}_1\tilde{u}_3}$ by diffusing and shifting the critical layer up and down (Hsu *et al.*, 1981); the consequences are that most of $-\overline{\tilde{u}_1\tilde{u}_3}$ is produced at the lower edge of the logarithmic profile where the curvature of the mean flow is large. This implies that $\overline{\tilde{u}_1\tilde{u}_3}(x_3^*)$ may change drastically near the interface. As a result, we expect that the measurement of $-\overline{\tilde{u}_1\tilde{u}_3}$ at the height as made in this experiment may be too small to provide values of $(-\overline{\tilde{u}_1\tilde{u}_3})_{\delta_0}$. We also expect that $(-\overline{\tilde{u}_1\tilde{u}_3})_{\delta_0}$ is considerably larger than that predicted based on a nonturbulent, linear, critical-layer model.

It remains to discuss the wave-induced pressure $\tilde{p}$ which is the most relevant quantity for the estimate of $\bar{M}_{w1}$. A measurement of the wave-induced pressure simultaneously in the fixed and wave-following frames was carried out by Snyder *et al.* (1981) for ocean waves. The elevation of their probe was $x_3 = h = 1$ m, which gave a nominal value of k_0h of 1.0 where k_0 is the wavenumber of the dominant wave. Agreement between their fixed and wave-following frames results was found after the results were extrapolated to the surface. The wave-induced pressures $\tilde{p}$ in the two frames are related by

$$\tilde{p}(x_1, x_2, x_3, t)|_{x_3=h} = \tilde{p}(x_1, x_2, x_3^*, t)|_{x_3^*=h} - f\tilde{\eta}\left.\frac{\partial\bar{p}}{\partial x_3}\right|_{x_3^*=h} \tag{5.5}$$

to the first order in wave slope. It is generally assumed that $\bar{p}$ remains quite constant in the boundary layer; this suggests that the measurement of $\bar{p}$ at $x_3 = h$ and at $x_3^* = h$ should be consistent. However, an extrapolation to the surface is required since $\bar{p}$ changes with elevation. It should be noted that the extrapolation to the interface represents the inviscid limit of $k_0\delta_0 \to 0$, i.e., the extrapolated results have to be interpreted as applying just outside the viscous sublayer.

6. Data reduction

A mean quantity $\bar{g}$ was deduced by the traditional time average defined as

$$\bar{g}(x) = \lim_{T\to\infty} \frac{1}{T}\int_{-T/2}^{T/2} g(x, t)dt, \tag{6.1}$$

where $g(x, t)$ is any quantity of interest. The correlation of g to a reference h is then $\overline{h(t)g(t+\xi)}$ where ξ represents the time separation during time averaging. Consequently, the cross-spectral density of g to h is defined as the Fourier transform of the cross correlation, i.e.,

$$\Phi_{gh}(f) = \int_{-\infty}^{\infty} \overline{h(t)g(t+\xi)}e^{i2\pi f\xi}d\xi, \tag{6.2}$$

$$= C_{gh}(f) + iQ_{gh}(f), \tag{6.3}$$

where $C_{gh}(f)$ is the co-spectral density and $Q_{gh}(f)$ is the quadrature spectral density. In actual computation, the integration bounds $\pm\infty$ in (6.2) are replaced by $\pm T/2$ with T made sufficiently large. Practically, T is divided into several segments, say, $T' = T/n$. From (6.2), it can be shown that

$$\Phi_{gh}(f) = \langle\langle G(f)H^*(f)\rangle\rangle df, \tag{6.4}$$

where $df = 1/T' = n/T$ denotes the resolution of the frequency spectrum, $G(f)$ and $H(f)$ are the Fourier transforms of $g(t)$ and $h(t)$ for each segment, the asterisk denotes a complex conjugate and the double angle braces represent the ensemble average over the n ensembles. Dividing T and nT' reduces the uncertainty of the analysis but increases the bandwidth of frequency resolution from $df = 1/T$ to n/T. In this study we choose $n = 50$ so that $df = 0.078$ Hz when $T = 10.7$ min.

The auto-spectral density is obtained by letting $g = h$, i.e.,

$$S_h(f) = \Phi_{hh}(f) = \langle\langle HH^*\rangle\rangle df = C_{hh}(f). \tag{6.5}$$

Clearly, $Q_{hh}(f) = 0$ because HH^* is real. Since the Fourier transform of $\partial h/\partial t$ is $-i2\pi fH(f)$, the cross-spectral density of g to $\partial h/\partial t$ is $i2\pi f\Phi_{gh}(f)$.

By letting $h = \tilde{\eta}$, the auto-spectral density of $\tilde{\eta}$ and the cross-spectral density between $\tilde{g}$ and $\tilde{\eta}$ can be found since $\Phi_{g\tilde{\eta}}(f) = \Phi_{\tilde{g}\tilde{\eta}}(f)$ from the assumption that $\bar{g}$ and g' are not correlated to $\tilde{\eta}$. However, the auto-spectral density and the cross-spectral density of wave-induced flowfields cannot be obtained directly from these expressions because the wave-induced quantity is random and cannot be separated from the turbulence. As the wave-induced component $\tilde{g}$ in the air flow quantity $g = \bar{g} + \tilde{g} + g'$ is defined to be perfectly correlated to $\tilde{\eta}$, we have in the frequency domain (Benilov, *et al.* 1974)

$$\tilde{G}(f) = \lambda_{\tilde{g}}(f)\tilde{Z}(f), \tag{6.6}$$

where $\tilde{G}$ and $\tilde{Z}$ are the Fourier transforms of $\tilde{g}$ and $\tilde{\eta}$ and $\lambda_{\tilde{g}}$ is the linear operator which describes the response of the air flow to $\tilde{\eta}$. Here, $\lambda_{\tilde{g}}$ is stationary and is a function of x_3. When (6.6) is multiplied by $\tilde{Z}^*$ and an ensemble average is taken, we find

$$\lambda_{\tilde{g}}(f) = \Phi_{\tilde{g}\tilde{\eta}}(f)/S_{\tilde{\eta}}(f). \tag{6.7}$$

Consequently, from (6.4), (6.6) and (6.7)

$$\Phi_{\tilde{g}\tilde{h}}(f) = \Phi_{\tilde{g}\tilde{\eta}}(f)\Phi_{\tilde{\eta}\tilde{h}}(f)/S_{\tilde{\eta}}(f), \tag{6.8}$$

where $\tilde{h}$ is another wave-induced quantity. Clearly, the auto-spectral density of $\tilde{g}$ can be obtained by letting $\tilde{h} = \tilde{g}$ in (6.8). This scheme is used to calculate $\overline{\tilde{u}_1\tilde{u}_3}$ and then $\overline{u'_1u'_3}$ is obtained by subtracting $\overline{\tilde{u}_1\tilde{u}_3}$ from $\overline{(\tilde{u}_1 + u'_1)(\tilde{u}_3 + u'_3)}$.

In computing the energy transfer, we have used the interface boundary value $\partial\tilde{\eta}/\partial t + \bar{u}_0\partial\tilde{\eta}/\partial x_1$ for $(\tilde{u}_3)_0$ rather than the value of $\tilde{u}_3$ measured at 5 mm above the highest wave crest because the direct measurements do not provide a reliable result for $(\tilde{u}_3)_0$ according to the observations of Hsu and Hsu (1982). The inclusion of the drift current $\bar{u}_0$ is substantial for a wind-generated wavefield in a laboratory since $\bar{u}_0$ is comparable to the wave celerity.

In evaluating the momentum transfer to waves, the Fourier transform for $\partial\tilde{\eta}/\partial x_1$ must be determined. The Fourier transform of $\partial\tilde{\eta}/\partial x_1$ derived from the Fourier transform of $\partial\tilde{\eta}/\partial t$ is dependent on the dispersion relation between the frequency f and the wavenumber k. The thin vortical wind-induced drift current usually has little influence on the wave propagation speed c (Phillips, 1977, p. 164). The laboratory measurements by Ramamonjiarisoa and Coantic (1976) and by Lake and Yuen (1978) show that the wave celerity c is given by

$$c = \begin{cases} \dfrac{g}{2\pi f}, & \text{if } f \leqslant f_0 \\ \dfrac{g}{2\pi f_0}, & \text{if } f > f_0, \end{cases} \tag{6.9}$$

where f_0 is the dominant wave frequency and g the gravitational acceleration. With (6.9) and $kc = 2\pi f$, the Fourier transform of $\partial\tilde{\eta}/\partial x_1$ can be obtained from the Fourier transform of $\partial\tilde{\eta}/\partial t$.

The directional distribution of the wind-wave field also gives a spreading factor

TABLE 1. Mean free stream velocity U_∞, friction velocity u_*, dominant-wave speed c_0, wave steepness $k_0\bar{a}$, and wave-speed-to-surface-drift-current-velocity ratio $c_0/\bar{u}_0$.

Run	Fetch (x_1) (m)	U_∞ (m s^{-1})	u_* (m s^{-1})	c_0 (m s^{-1})	$\bar{a}$ (mm)	$k_0\bar{a}$	c_0/u_*	$c_0/\bar{u}_0$
	3.46	6.76	0.283	0.283	2.12	0.258	1.00	1.81
	6.51	6.92	0.315	0.375	4.05	0.281	1.19	2.16
I	9.48	7.02	0.326	0.460	5.51	0.256	1.41	2.56
	12.61	7.09	0.336	0.521	6.75	0.244	1.55	2.82
	15.66	7.26	0.353	0.600	8.31	0.226	1.70	3.09
	3.46	7.62	0.342	0.301	2.70	0.293	0.88	1.60
	6.51	7.73	0.362	0.409	5.03	0.293	1.13	2.05
II	9.48	7.90	0.408	0.490	6.77	0.279	1.20	2.18
	12.61	8.01	0.400	0.580	8.70	0.255	1.45	2.64
	15.66	8.10	0.424	0.649	9.83	0.228	1.53	2.78
	3.46	8.43	0.405	0.348	3.82	0.310	0.86	1.56
	6.51	8.62	0.414	0.451	6.02	0.288	1.09	1.98
III	9.48	8.81	0.475	0.556	8.45	0.267	1.17	2.13
	12.61	8.88	0.484	0.639	9.99	0.242	1.32	2.40
	15.66	8.97	0.487	0.711	11.27	0.220	1.46	2.65

$$\int_{-\pi/2}^{\pi/2} D'(\theta)\cos\theta d\theta = 128/(45\pi)$$

to the correlation $\overline{\tilde{g}\partial\tilde{\eta}/\partial x_1}$ because the wave number in the x_1 direction is $k\cos\theta$. Thus,

$$\overline{\tilde{g}\frac{\partial\tilde{\eta}}{\partial x_1}} = \frac{256}{45\pi}\int_0^\infty kQ_{\tilde{g}\tilde{\eta}}(f)df.$$

In order to evaluate the transfer by $\tilde{r}_{ij}$, the Fourier transform for $\tilde{u}_i\tilde{u}_j - \bar{\tilde{u}}_i\bar{\tilde{u}}_j$ was obtained by performing the convolution between the Fourier transforms u_i and u_j and requiring the resultant spectrum to be zero at zero frequency. The result is then subtracted from the Fourier transform of $(\tilde{u}_i + u_i')(\tilde{u}_j + u_j') - (\bar{\tilde{u}}_i + u_i')(\bar{\tilde{u}}_j + u_j')$. The difference is the Fourier transform of $\tilde{r}_{ij}$ and can be correlated directly to the Fourier transforms of $\partial\tilde{\eta}/\partial x_1$, $\tilde{u}_1$ and $\tilde{u}_3$ for the evaluation of the momentum and energy transfer.

7. Experimental results

a. Characteristics of the wind and the waves

The mean free stream velocities for the three runs at different fetches are shown in Table 1. Fig. 1 shows the mean velocity profiles measured by the Pitot-static tube. There is wake behavior near the free stream. When the wind speed is higher, the elevation where the wake effect begins to be felt is lower. At the wind speeds of this study, the lowest portion of the profile, as seen from Fig. 1, may be only marginally free from the wake effect. Consequently, the friction velocity u_* determined by the profile method (using even the lowest portion of the mean velocity profile) is too high. On the other hand, Hsu *et al.* (1981) showed that when the wind speed is low, the value of $(-\overline{u_1'u_3'})^{1/2}$ determined from a turbulent measurement of the constant stress layer was in excellent agreement with the u_* obtained by profile method. The results of Hsu *et al.* also showed that the constant turbulent shear layer extends up to $x_3/\delta = 0.4$ where δ is the thickness of the turbulent boundary layer. As the turbulence measurement made in this study was at elevations lower than the lowest elevations of each Pitot-static tube measurement and was in the constant mean turbulent shear layer, we shall discard the profile method and use $u_* = (-\overline{u_1'u_3'})^{1/2}$ to determine u_*. The values of u_* thus obtained are also given in Table 1. The thickness of viscous sublayer estimated by $\delta_0 u_*/\nu = 10$ (Phillips, 1977, p. 128) is less than 0.57 mm.

The drag coefficient C_D determined by $C_D = (u_*/U_\infty)^2$ is plotted as a function of $U_\infty x_1/\nu$ (Fig. 2). Also included in Fig. 2 are the results reported by Hsu *et al.* (1982) for winds over mechanically-generated water waves measured also in the Stanford wind/wave channel. For comparisons, the curves for boundary layer flow over completely rough and smooth plates (Schlichting, 1968) are also shown in Fig. 2. As reasoned by Hsu *et al.* (1982), the increase in C_D with increasing $U_\infty x_1/\nu$ results from the increase in surface roughness associated with the wind-generated waves. However, we observed that C_D for the wind-generated waves is higher than that for the mechanically-generated waves at comparable values of $U_\infty x_1/\nu$. This is consistent with the phenomenon of short-wave suppression by longer waves or swell as observed by Mitsuyasu (1966) and analyzed by Phillips and Banner (1974). The suppression of short waves by mechanically-generated waves results in a decrease in surface roughness and consequently in C_D.

The wind wave spectra for the three runs are shown in Fig. 3. The growth of the waves, the shifting of the

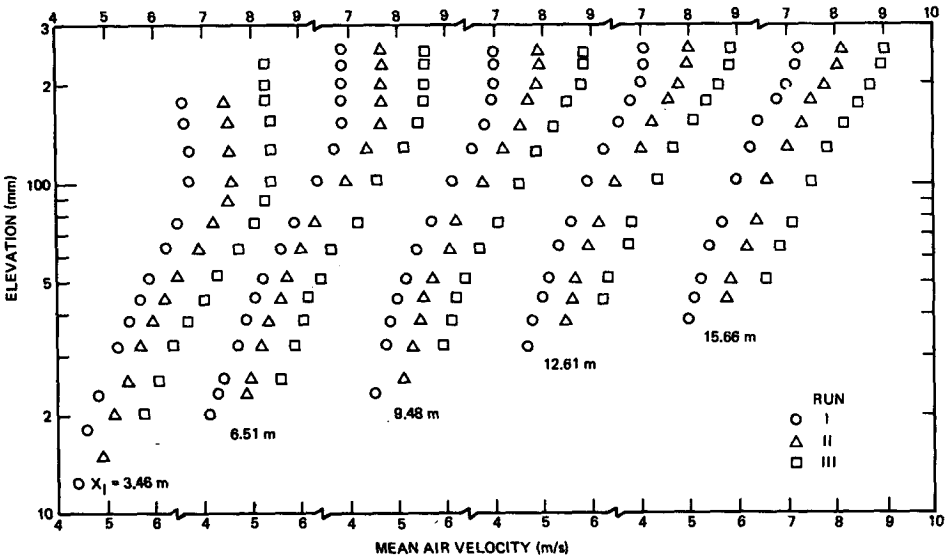

FIG. 1. Mean air velocity profiles at fetches of 3.46, 6.51, 9.48, 12.61 and 15.66 m for Runs I, II, III.

dominant wave to a lower frequency range as a function of increasing x_1, and the overshoot phenomenon [as observed by Barnett and Sutherland (1968)] are evident. The second harmonic forced component located at twice the dominant wave frequency is relatively strong, indicating the wave field is quite nonlinear. In Fig. 3, we also find a lower hump at frequencies below 2 Hz. This lower hump is contributed from the waves reflected from the beach and is less than 2% of the dominant wave. Hence, the effect of beach reflection is negligible. The wave celerity c_0 for the dominant waves is calculated from (6.9) based on the observed f_0; the value c_0 as well as the ratio c_0/u_* are given in Table 1. The total energy $\overline{\tilde{\eta}^2}$ can be obtained by the integration of the spectral density with respect to f or by taking the variance of $\tilde{\eta}$. The mean wave amplitude $\bar{a}$ is defined as [see also Eq. (2) of Yuen and Lake (1979)]

$$\bar{a} = (2\overline{\tilde{\eta}^2})^{1/2}. \tag{7.1}$$

The values of $\bar{a}$ and $k_0\bar{a}$, where k_0 is the dominant wavenumber obtained in this experiment, are listed in Table 1.

The development of the wind waves in terms of the normalized total wave energy $\hat{E}$ $(=\overline{\tilde{\eta}^2}g^2/u_*^4)$ and the normalized dominant wave frequency $\hat{f}_0(=f_0u_*/g)$ as functions of the dimensionless fetch $\hat{x}$ $(=x_1g/u_*^2)$ are shown in Fig. 4; they are in reasonably good agreement with the measurements carried out both in the ocean and laboratory (Hasselmann *et al.*, 1973, 1976). For additional details the reader can refer to Phillips (1977, p. 159). The empirical relations for $\hat{f}_0$ and $\hat{E}$ in the laboratory are

$$\hat{f}_0 = 1.0\hat{x}^{-1/3}, \tag{7.2}$$

$$\hat{E} = 1.6 \times 10^{-4}\hat{x}. \tag{7.3}$$

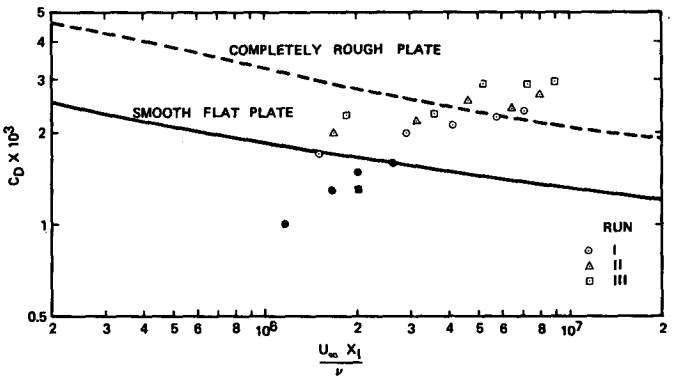

FIG. 2. Wind drag coefficient C_D as a function of Reynolds number $U_\infty x_1/\nu$ for Runs I, II, III and (●) Yu *et al.* (1973) and (■) Hsu *et al.* (1981).

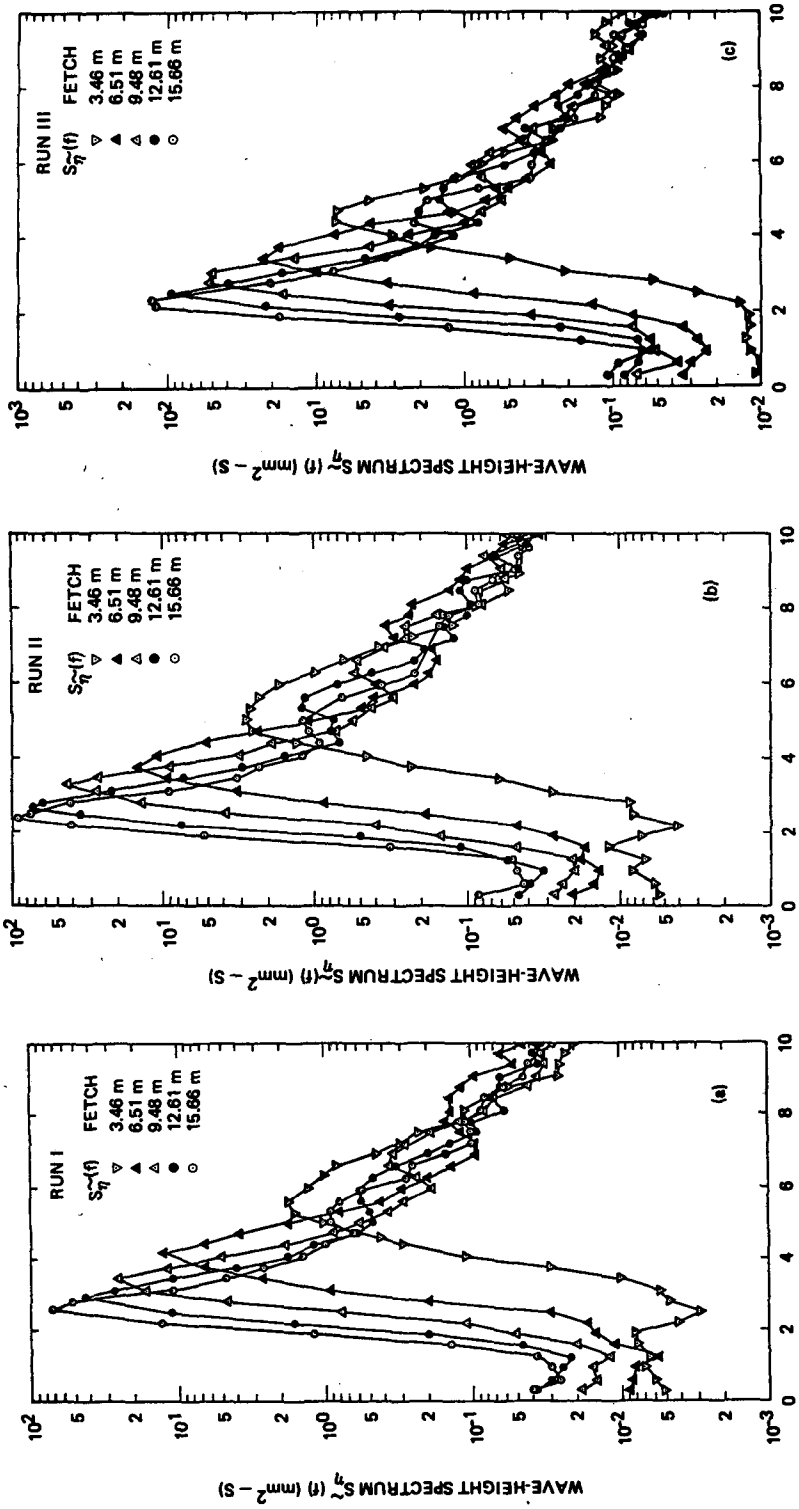

FIG. 3. Power spectral density of wave amplitudes as developing with fetch for different winds. (a), (b) and (c) are for Runs I, II and III, respectively.

Since $u_*/c_0 = 2\pi\hat{f}_0$, the elimination of $\hat{x}$ from (7.2) and (7.3) leads to

$$k_0\bar{a} = 0.282(c_0/u_*)^{-1/2}. \tag{7.4}$$

On the other hand, for the ocean, the empirical relation for $\hat{f}_0$ is best given by [Eq. (4.6.2) of Phillips (1977)]

$$\hat{f}_0 = 0.35\hat{x}^{-1/4}, \tag{7.5}$$

while (7.3) for $\hat{E}$ remains applicable. Elimination of $\hat{x}$ from (7.3) and (7.5) results in $k_0\bar{a}$ = constant = 0.087 for the field data. A plot of $k_0\bar{a}$ as a function of c_0/u_* is given in Fig. 5. Our present experimental results are in good agreement with (7.4). For comparisons, the field observations by Snyder *et al.* (1981) and the JONSWAP data by Müller (1976) are also shown in Fig. 5. Although (7.4) seems to describe the field results reasonably well, a better interpretation of the dependence of $k_0\bar{a}$ on c_0/u_* is found from the nonlinear wind-waves model of Lake and Yuen (1978) and Yuen and Lake (1979); the details of this are discussed in Section 8.

b. The wave-induced flowfields

The wave-induced flow quantity is characterized by the power spectral density, as well as by the coherence and the phase lag angle to the surface waves. Because each case (at different fetches and/or wind speeds) shows similar results, for the purpose of demonstrating the characteristics of the wave-induced flow only the results for Run III (U_∞ = 8.97 m s^{-1}) at x_1 = 15.66 m are presented here. For results of lower wind speeds and/or fetches, the reader is referred to Wu *et al.* (1977).

The power spectral densities of $\tilde{p}$, $\tilde{u}_1$ and $\tilde{u}_3$ are shown in Fig. 6a, and their coherences and phase lag angles to $\tilde{\eta}$ in Figs. 6b and 6c, respectively. As shown in Fig. 6a, the power spectral densities of $\tilde{p}$, $\tilde{u}_1$ and $\tilde{u}_3$ have shapes similar to that of the wave height spectrum. Therefore, the flowfield near the interface is strongly coupled with the interfacial wave motion. However, the correlation of the air flow to the surface waves seem to be confined to the frequency bands near the frequencies of the dominant wave and its harmonics, since the amplitudes of $\tilde{p}$, $\tilde{u}_1$ and $\tilde{u}_3$ in the frequency range between two adjacent harmonics are relatively low. This phenomenon is more clear for the pressure. The phenomenon is also evident from the coherence and phase angle spectra shown in Figs. 6b and 6c.

Since the wave-induced component $\tilde{g}$, where $\tilde{g}$ can be $\tilde{p}$, $\tilde{u}_1$ or $\tilde{u}_3$, is defined to be completely correlated to $\tilde{\eta}$, the coherence between $\tilde{g}$ and $\tilde{\eta}$ should be equal to 1. The loss of correlation between $\tilde{g}$ and $\tilde{\eta}$ at higher frequency as shown in Fig. 6b implies that our signal-to-noise ratio decreases when the frequency increases. As a result, the ensemble average applied to reduce

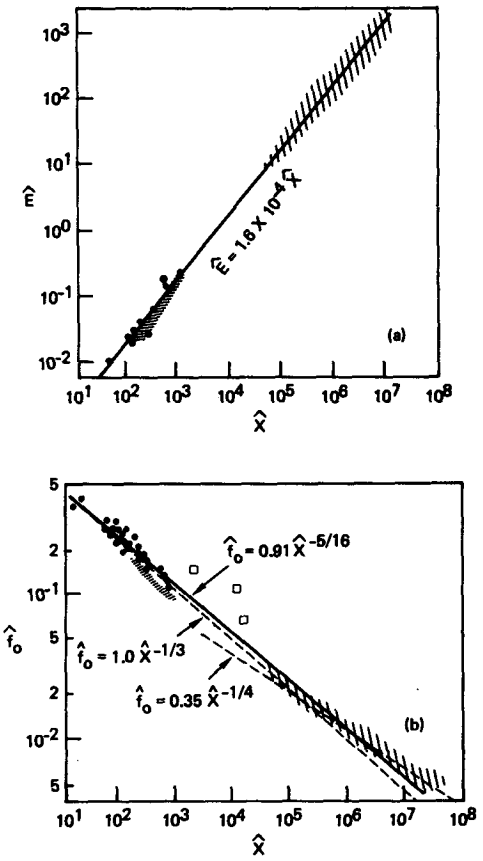

FIG. 4. Developments of (a) wave energy and (b) peak frequency as function of fetch. (●) Mitsuyasu (1968); (⊡) Hidy and Plate (1966); vertical hatching, Hasselmann *et al.* (1973); horizontal hatching, this experiment.

$\Phi_{\tilde{g}\tilde{\eta}}(f)$ is not sufficient in eliminating $G'(f)$ completely from $G(f) + G'(f)$ at higher frequency, where $G'(f)$ is the Fourier transform of g'. This loss of correlation occurs 1) because the turbulent spectrum is relatively flat in the lower frequency range and decreases at most as $f^{-5/3}$ in the higher frequency range while the wind wave spectrum decreases as rapidly as f^{-5}, and 2) because the wave-induced components at higher frequency have a smaller length scale and, hence, decay more rapidly in the x_3 direction than do the lower frequency components. However, the very low coherence at the frequency range between two adjacent harmonics indicates the response of air flow to $\tilde{\eta}$ is very small there. Consistency is also found from the phase of $\tilde{g}$; $\tilde{g}$ has an almost constant phase relation to $\tilde{\eta}$ near the frequencies of the dominant wave and its harmonics, but not in between. The results suggest that the wave-induced flow tends to behave as forced waves and that the surface waves may contain strong components of forced waves. Our present data seem to support the nonlinear wind waves model proposed by Lake and Yuen (1978) and Yuen and Lake (1979).

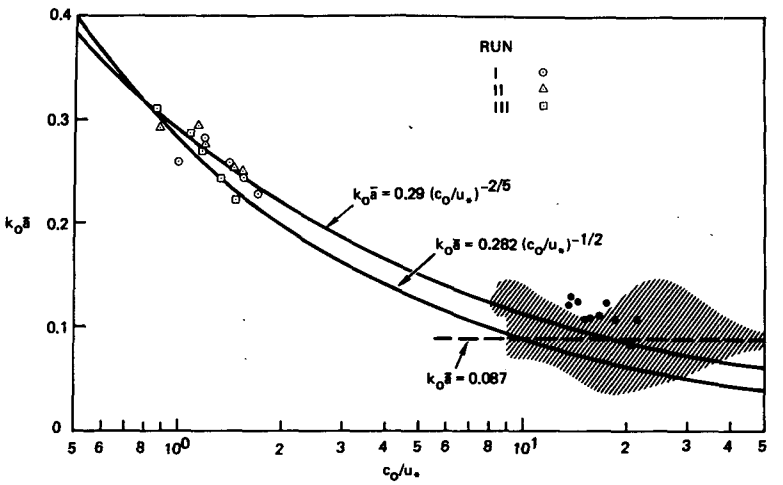

FIG. 5. The steepness of the dominant wave of wind-generated waves as a function of the wind/waves coupling parameter c_0/u_* for Runs I, II and III; and (●) Snyder *et al.* (1981); and hatching, JONSWAP data of Müller (1976).

c. Momentum and energy budget

The stress spectrum $\tau_w(f)$ $[=(4\pi f/c)Q_{\tilde{p}\tilde{\eta}}(f)]$ and the energy input spectrum $S_{in}(f)$ $[=4\pi f Q_{\tilde{p}\tilde{\eta}}(f)]$ due to the action of the wave-induced pressure are shown in Fig. 7. Again, the results are only for Run III (U_∞ = 8.97 m s^{-1}) at x_1 = 15.66 m and the results for lower wind speeds and/or fetches are not presented since they are all similar. The important phenomenon is that the momentum and energy transfer from wind to waves by the wave-induced pressure occurs mainly in the frequency range near the dominant wave. The integration of the spectra shown in Fig. 7 with respect to f shows that more than 90% of the momentum and energy transfer is contained in a frequency rage $0.5 < f/f_0 < 1.5$.

Table 2 provides the momentum budget to the current and the wave fields. As shown in Table 2, the ratio γ_M of momentum flux $\bar{M}_{w1}$ supported by the waves to the total momentum flux $\bar{M}_1$ across the interface increases with increasing fetch. This is expected since with increasing fetch the increase in $\bar{M}_{c1}(=\rho u_*^2)$ due to boundary layer development is relatively weak compared to the increase in $\bar{M}_{w1}$ due to the development of the wavefield. There is an apparent weak increase in γ_M with increasing wind velocity, but this is not clear as the fetch dependence because both $\bar{M}_{c1}$ and $\bar{M}_{w1}$ change as functions of u_*^2. The average value of γ_M is 0.61. The contribution to $\bar{M}_{w1}$ by turbulent transfer $\rho\tilde{r}_{11}\partial\tilde{\eta}/\partial x_1$ is found to be approximately 27%.

To evaluate the energy budget to the current and the wave fields, information about the surface drift current velocity is required. In this study, we did not measure the surface current velocity. As a result, we use the data measured by others to infer the surface current velocity for this study. Surface currents were measured by Keulegan (1951), Wu (1968, 1975) and Phillips and Banner (1974). Based on these measurements, the surface current velocity $\bar{u}_0$ was found to be related to u_* by $\bar{u}_0 = 0.55u_*$ (Phillips, 1977, p. 92). The values of $\bar{u}_0$ thus determined using the measured u_* of this experiment are given in ratio $c_0/\bar{u}_0$ in Table 1. Since the surface current is difficult to measure with good accuracy, our estimate of $\bar{u}_0$ is expected to have the same accuracy as that of a direct measurement.

The energy transfer rates shown in Table 3 indicate that the ratio γ_E of energy flux to the waves ($\bar{E}_w$) to the total energy flux across the interface ($\bar{E}_{ii}$) shows more scatter than γ_M. However, apparently γ_E increases somewhat with fetch, but has no systematic dependence on the wind speed. The average γ_E is 0.29. The direct energy transfer to the waves by turbulence is dominated by $-\rho\tilde{r}_{13}$, but is only about 30% of the transfer by the wave-induced pressure. The negative sign in the turbulent transfer indicates that our calculations suggest that the energy is being drawn from the water wave field to the wind turbulence. However, the uncertainty associated with the determination of the turbulent transfer is high. In spite of this, it is still safe to say that the momentum and energy transfer to waves is dominated by the wave-induced pressure.

The direction of energy transfer by $\tilde{r}_{13}$ is different from that obtained by Hsu *et al.* (1982) for wind over a smooth mechanically-generated water wave. They found, in addition, that the turbulence contributes less than 5% of the energy transfer to waves. The higher percentage for the direct turbulent transfer in this present study may be due to a higher turbulent intensity associated with the higher surface roughness of the short waves in the wind wave spectrum (see Fig. 2). The role of surface roughness played by the

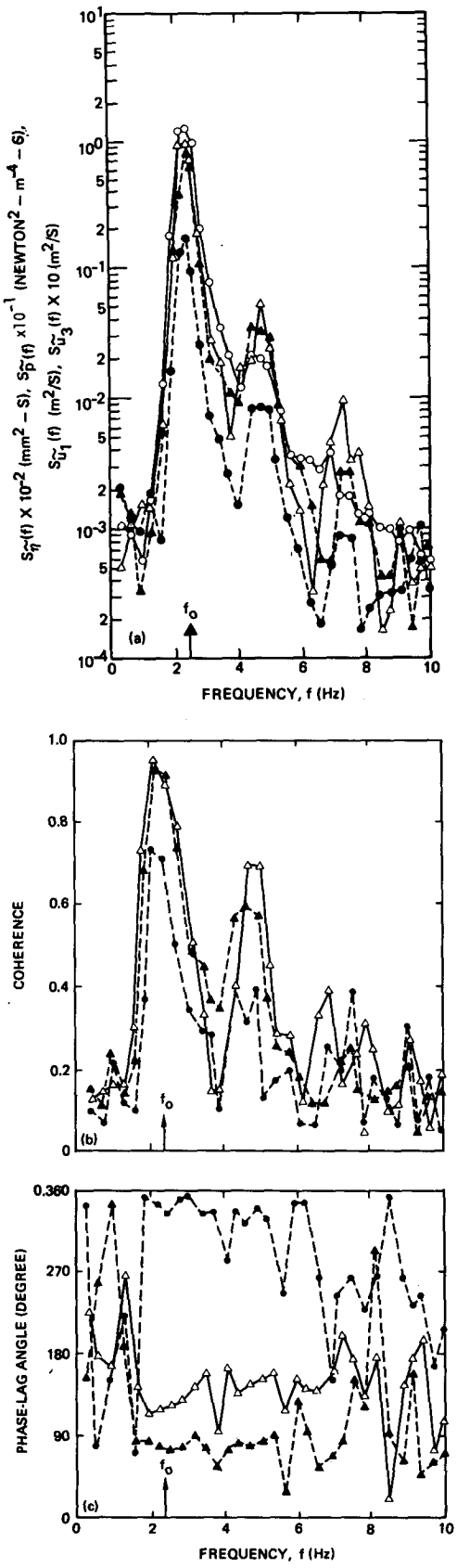

short waves is also significant to the turbulent Reynolds stresses perturbed by the dominant wave. The predictions by Gent and Taylor (1976) for flows over water waves with surface roughness showed that the maximum of $-\tilde{r}_{13}$ occurs at the windward side of the wave slope and has a phase difference of about 180° from the observation of Hsu *et al.* (1981, 1982). This may explain the difference in the direction of the energy transfer by $\tilde{r}_{13}$ between this study and that of Hsu *et al.* (1982).

d. Developing wind waves

The measured wind waves development was presented in Section 7a and the measured energy input from wind to waves was given in Section 7c. Here, we attempt to give insight to the developing wind wave process resulting from wind energy input. We base our descriptions on the nonlinear wind wave model proposed by Lake and Yuen (1978) and Yuen and Lake (1979, 1980). A brief description of the nonlinear wind wave model is essential: (i) the wind waves are locally characterized by a single wave train with a "carrier" frequency equal to the dominant wave frequency; (ii) a developing wind wave system is a bound wave system whose spectral components result mainly from the modulation and demodulation of the nonlinear dominant wave train; (iii) short waves are free waves, but contain negligible energy and do not affect directly the dynamical properties of the developing wind waves field; (iv) the evolution of the nonlinear wind waves to the first approximation is characterized by the nonlinear Schrödinger equation which under the influence of wind energy input leads to the growth of the spectral peak and the continuous down-shifting of the dominant wave frequency.

The most significant feature in the energy input mechanism for the nonlinear wind waves is that the wind energy input is mainly to the dominant wave. This was postulated originally by Deardorff (1967) and adopted by Lake and Yuen (1978), and is confirmed by this experiment (see Figs. 3 and 7). The ripples (short waves) do not affect the nonlinear characteristics of the dominant wave, but may change the wave-induced flow as described by surface roughness associated with ripples. For the nonlinear wind wave model, the nonlinear wave-wave interaction associated with a free wave system (Hasselman, 1962, 1963, 1966, 1967) is ignored since the modulation of the nonlinear wave train due to Benjamin-Feir (1967)

FIG. 6. The spectra of wave-induced airflow quantities at a fetch of 15.66 m and wind speed of 8.97 m s^{-1} (Run III). (a) Power spectral density; (b) coherence with waves; (c) phase angle lag to waves. The wave-induced quantities are: (△), $\tilde{p}$; (●) $\tilde{u}_1$; (▲) $\tilde{u}_3$. For comparisons, the power spectral density of the surface water waves (○) is also included in (a).

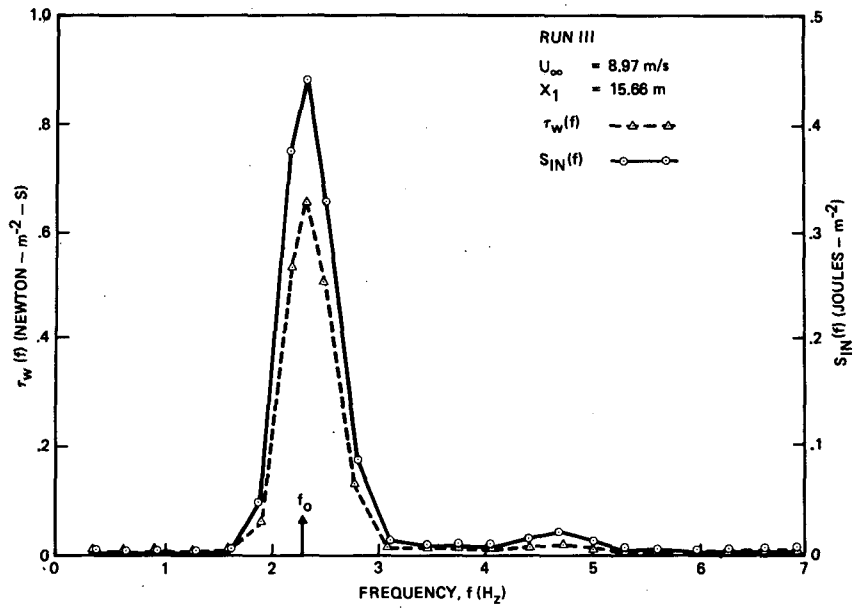

FIG. 7. Spectral density of momentum $\tau_w(f)$ and energy $S_{in}(f)$ transfer to waves due to wave-induced pressure acting at a fetch of 15.66 m for a wind speed of 8.97 m s^{-1} (Run III).

instability and the demodulation due to Fermi-Pasta-Ulam (FPU) recurrence as described by Lake *et al.* (1977) take the essential role of describing the wave evolution. The energy transfer mechanism proposed by Wu (1972), namely, the wind transfers energy mainly to short waves and then the nonlinear wave-wave interaction transfers the energy in the short waves to the dominant waves for the wave growth, is not applicable here although under some ocean wave conditions this mechanism might still be appropriate.

The change in the wave energy as a result of wind energy input can be written as

$$\frac{\partial}{\partial t}(\overline{\tilde{\eta}^2}) = \frac{1}{\rho_w g}\bar{E}_w\,, \tag{7.6}$$

TABLE 2. Momentum budget between the turbulent boundary layer winds and the wind-generated water waves.

Run	Fetch (m) x_1	Momentum transfer rates ($\times 10$ N m^{-2}) $\overline{\tilde{p}\frac{\partial\tilde{\eta}}{\partial x_1}}$	$\overline{\rho\tilde{r}_{11}\frac{\partial\tilde{\eta}}{\partial x_1}}$	$\overline{-\tilde{\tau}_{11}\frac{\partial\tilde{\eta}}{\partial x_1}}$	$-\overline{\rho u_1' u_3'}$	$\bar{M}_{w1}$	$\bar{M}_1$	Transfer ratios γ_t[a]	γ_M
	3.46	0.44	0.16	0.0038	0.97	0.60	1.57	0.27	0.38
	6.51	0.99	0.37	0.0044	1.20	1.37	2.57	0.27	0.53
I	9.48	1.40	0.37	0.0033	1.29	1.77	3.06	0.21	0.58
	12.61	1.33	0.67	0.0040	1.37	2.00	3.38	0.33	0.59
	15.66	2.11	0.62	0.0049	1.51	2.73	4.24	0.23	0.64
	3.46	1.12	0.16	0.0067	1.42	1.29	2.70	0.12	0.48
	6.51	1.72	0.15	0.0066	1.58	1.87	3.45	0.08	0.54
II	9.48	2.14	1.42	0.0061	2.02	3.56	5.59	0.40	0.64
	12.61	2.98	2.52	0.0063	1.94	5.51	7.45	0.46	0.74
	15.66	3.70	2.25	0.0068	2.18	5.96	8.14	0.38	0.73
	3.46	2.40	0.58	0.0101	1.99	2.98	4.97	0.19	0.60
	6.51	2.85	0.16	0.0079	2.08	3.01	5.09	0.06	0.59
III	9.48	3.75	1.57	0.0089	2.73	5.33	8.06	0.29	0.66
	12.61	4.65	2.60	0.0094	2.84	7.26	10.10	0.36	0.72
	15.66	5.79	2.98	0.0100	2.87	8.78	11.65	0.34	0.75
							Average	0.27	0.61

[a] $\gamma_t = \left(\overline{\rho\tilde{r}_{11}\frac{\partial\tilde{\eta}}{\partial x_1}}\right)\Big/\bar{M}_{w1}$, the partition of momentum transfer to waves by wave-induced turbulent Reynolds stress $\rho\tilde{r}_{11}$.

TABLE 3. Energy budget between the turbulent boundary layer winds and the wind-generated water waves.

Run	Fetch (m) x_1	Energy transfer rates ($\times$ 10 J m^{-2} s^{-1}) $-\overline{\tilde{p}\tilde{u}_3}$	$-\overline{\rho\tilde{r}_{13}\tilde{u}_1}$	$-\overline{\rho\tilde{r}_{33}\tilde{u}_3}$	$\rho\bar{r}_{13}\overline{\frac{\partial\tilde{\eta}}{\partial x_1}\tilde{u}_3}$	$\bar{M}_1\bar{u}_0$	$\bar{E}_w$	$\bar{E}_{ii}$	Transfer ratio γ_E
	3.46	0.07	−0.016	−0.008	0.005	0.25	0.05	0.29	0.17
	6.51	0.24	−0.022	0.002	0.010	0.45	0.23	0.68	0.34
I	9.48	0.46	−0.15	−0.040	0.015	0.55	0.29	0.84	0.34
	12.61	0.52	−0.20	−0.046	0.018	0.62	0.29	0.92	0.32
	15.66	0.99	−0.32	0.009	0.020	0.82	0.70	1.52	0.46
	3.46	0.16	−0.048	−0.020	0.013	0.51	0.11	0.61	0.17
	6.51	0.43	−0.13	−0.040	0.018	0.69	0.28	0.97	0.29
II	9.48	0.68	−0.40	−0.13	0.032	1.25	0.18	1.43	0.13
	12.61	1.25	−0.46	−0.20	0.039	1.63	0.64	2.27	0.28
	15.66	1.79	−0.44	−0.17	0.040	1.90	1.22	3.12	0.39
	3.46	0.39	−0.16	−0.039	0.030	1.10	0.22	1.32	0.17
	6.51	0.77	−0.19	−0.034	0.034	1.16	0.58	1.74	0.33
III	9.48	1.32	−0.60	−0.17	0.065	2.11	0.62	2.73	0.23
	12.61	2.04	−0.57	−0.38	0.077	2.69	1.16	3.85	0.30
	15.66	2.99	−0.98	−0.19	0.069	3.12	1.89	5.01	0.38
								Average	0.29

where $\bar{E}_w$ is given by (4.5) and ρ_w is the density of water. Based on the nonlinear wind wave model, the amplitude of the wave-induced pressure can be expressed to the first approximation as $\hat{p} = (\alpha + i\beta) \times \rho u_*^2(k_0\bar{a})$. Since $\tilde{u}_3 = \partial\tilde{\eta}/\partial t + \bar{u}_0\partial\tilde{\eta}/\partial x_1$ at the interface, we have

$$-\overline{(\tilde{p}\tilde{u}_3)_0} = \frac{1}{2}\rho\beta c_0 u_*^2(k_0\bar{a})^2\left(1 - \frac{128}{45\pi}\frac{\bar{u}_0}{c_0}\right). \quad (7.7)$$

A relation similar to (7.7) is postulated for the vertical transfer by turbulent stresses with a correction factor β_t denoting the ratio of the turbulent transfer to the transfer by $\tilde{p}$. Because $\tilde{u}_1 = k_0(c_0 + \bar{u}_0)\tilde{\eta}$ at the interface, the energy transfer by $\tilde{r}_{13}$ is then expressed as

$$-\rho\overline{(\tilde{r}_{13})_{\delta_0}(\tilde{u}_1)_0} = \frac{1}{2}\rho\beta\alpha_t c_0 u_*^2(k_0\bar{a})^2\left(1 + \frac{\bar{u}_0}{c_0}\right). \quad (7.8)$$

As a result, we find

$$\frac{\partial\hat{E}}{\partial\hat{x}} = s\beta(k_0\bar{a})^2\left[(1+\beta_t)\left(1 - 0.9\frac{\bar{u}_0}{c_0}\right) + \alpha_t\left(1 + \frac{\bar{u}_0}{c_0}\right)\right], \quad (7.9)$$

where $s = \rho/\rho_w = 0.0012$. Note that (7.9) reduces to Deardorff's (1967) form-drag model relation if $\alpha_t = \beta_t = \bar{u}_0 = 0$. Deardorff also assumed $k_0\bar{a}$ to be constant for developing wind waves and found $k_0\bar{a} = 0.177$ for moderate fetch ocean data collected by Wiegel (1967). Deardorff's predictions apparently agreed reasonably with the curves shown in Fig. 5 where, at moderate fetch of $3 < c_0/u_* < 6$, $k_0\bar{a}$ is $\sim$0.15.

In (7.9), the effect of turbulence on the wind energy input is illustrated in two ways: one is the direct energy transfer by turbulence characterized by α_t and β_t and the other is indirectly to alter the value of β associated with the transfer by $\tilde{p}$. Since the derivation of (7.9) is mostly based on dimensional argument, the determinations of α_t, β_t and β are most likely to be empirical. The energy budget shown in Table 3 suggests that $\alpha_t = -0.15$ and $\beta_t = -0.05$, while β is estimated in the following paragraph.

The evaluation of β has been the main issue in the past two decades in regard to the generation of waves by wind. According to Miles (1957, 1960), the wave growth parameter ζ due to the energy input by $\tilde{p}$ is expressed as

$$\zeta = \beta s(u_*/c_0)^2. \quad (7.10)$$

His predictions of β for logarithmic mean velocity profiles based on an inviscid quasi-laminar model showed that β depends strongly on the height x_{3c} of the critical layer and that the maximum β is 21 when $k_0x_{3c} = 0.01$. From Fig. 1 and Table 1, we have $k_0x_{3c} = 0.002$–0.01 for this experiment. Hence, β would be about 20 based on Miles' prediction. However, the values of c_0/u_* shown in Table 1 also imply that x_{3c} is less than the viscous sublayer thickness. The use of the logarithmic mean velocity profile in Miles' prediction becomes invalid because the mean profile becomes linear in the viscous sublayer. More exact numerical predictions of β, which include not only the linear profile of the viscous sublayer, but also the shear flow in the water, were given by Valenzuela (1976) and Kawai (1979). Their predictions are in good agreement with their experiment for initial wavelets of gravity-capillary waves. The significance of Miles' (1957, 1960) analyses lies not in the evaluation of β, but in the nondimensional form of (7.10) where

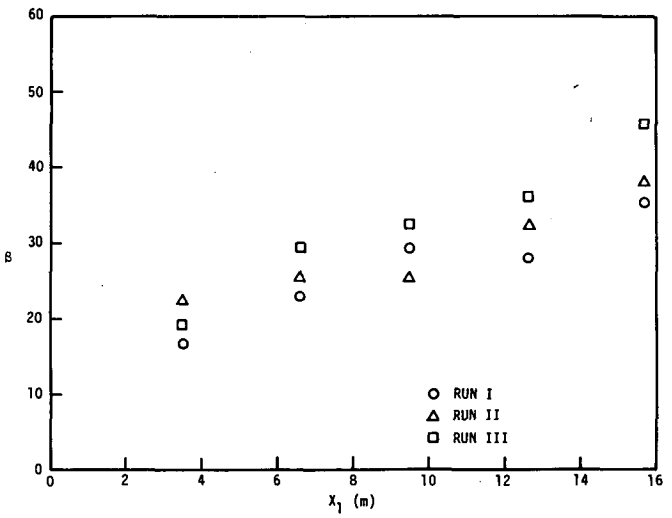

FIG. 8. Wave-induced pressure form drag coefficient β as a function of the fetch.

β then can be determined experimentally. The parameter ζ determined experimentally from the quadrature spectral density of $\tilde{p}$ and $\tilde{\eta}$ is

$$\zeta = \frac{Q_{\tilde{p}\tilde{\eta}}(f)}{\rho_w g S_{\tilde{\eta}}(f)}. \tag{7.11}$$

The results of ζ for this study as computed from (7.11) were compiled by Plant (1982) with laboratory results of Shemdin and Hsu (1967) and Larson and Wright (1975) and field results of Snyder *et al.* (1981). Plant (1982) found β range from 20 to 60. As a result, it appears that $\beta = 40$ is mostly correct for the existing data.

In the laboratory, our observations shown in Fig. 8 indicate that $\beta \approx 20$ at $x_1 = 3.46$ m and increases to about 40 at $x_1 = 15.66$ m, and that β increases slightly with increasing wind speed. This seems to be in contradiction to the implication by Plant (1982) where the variation in β is attributed to the uncertainty in measurement. An alternative explanation for the observed β shown in Fig. 8 can be offered if we examine the dependence of β on the wave slope (of the dominant wave) and on the surface roughness (associated with the short waves).

The dependence of β on the wave slope $k_0\bar{a}$ and on the surface roughness (relative to the wave length) k_0z_0 was demonstrated by Gent and Taylor (1976) and Gent (1977), and recently by Al-Zanaidi and Hui (1981). Gent and Taylor (1976) showed that the predicted β increases when u_*/c_0 increases, $k_0\bar{a}$ decreases or k_0z_0 decreases while the other two parameters are kept constants. This implies that

$$\beta = \beta(k_0\bar{a}, k_0z_0, u_*/c_0). \tag{7.12}$$

For the wind-generated waves, the dominant wave evolves along the fetch. Thus, all the three parameters in (7.12) change with the fetch and consequently are interdependent. Although the wind has the tendency to follow the dominant wave, the surface condition associated with the short waves is usually aerodynamically rough and z_0 is characterized by Charnock's (1955) relation $z_0g/u_*^2 = C_c$ where C_c is the Charnock's constant (Phillips, 1977, p. 194). Hence, we find $k_0z_0 = C_c(u_*/c_0)^2$. The computations by Gent (1977, Table 3) for $C_c = 2.1 \times 10^{-2}$ indicated that, when $k_0\bar{a}$ is fixed, the value of β remains practically constant for different c_0/u_*, i.e., the decrease in β due to the increase in k_0z_0 tends to balance the increase in β due to the increase in u_*/c_0. Hence, if we rewrite (7.12) as

$$\beta = \beta(k_0\bar{a}, C_c, u_*/c_0), \tag{7.13}$$

the dependence of β on u_*/c_0 according to the calculations of Gent (1977) is very weak and practically negligible. As a result, the observed dependence of β on fetch as shown in Fig. 8 may be a consequence of the dependence of β on $k_0\bar{a}$ which was shown in Section 7a to be indirectly a function of fetch.

The results of β as a function of $k_0\bar{a}$ are plotted in Fig. 9. Included also are the field observations by Snyder *et al.* (1981) and the numerical predictions by Miles (1960) [for $C_c = 6.3 \times 10^{-2}$, $c_0/u_* = 5$], by Gent (1977) [for $C_c = 2.1 \times 10^{-2}$], and by Al-Zanaidi and Hui (1981) [for $C_c = 2.1 \times 10^{-2}$, $c_0/u_* = 8$]. Apparently, the predictions of Al-Zanaidi and Hui (1981) are basically consistent with the observations. In view of the weak dependence of β on u_*/c_0, it is noted that a better agreement between the predictions and the observations can be obtained if Al-Zanaidi and Hui (1981) use a lower $C_c = 1.1 \times 10^{-2}$ as cited by Phillips (1977, p. 195), because both the computations of Miles (1960) and Gent (1977) indicated

that the lower the values of C_c the higher the results of β.

With this information about β, we now return to (7.9) and examine the rate of energy increase as a consequence of the wind energy input. Using α_t, β_t and β of this experiment, the right-hand side of (7.9) is evaluated as approximately equal to 8.2×10^{-4}. On the other hand, if we take $k_0\bar{a} = 0.087$, $\beta = 40$ and $\bar{u}_0/c_0 = 0$ as field conditions, we find the right-hand side of (7.9) is equal to 2.8×10^{-4}. These values are considerably larger than the empirical value 1.6×10^{-4} cited in (7.3) and shown in Fig. 4. However, it should not be taken seriously because (7.9) is primarily based on the assumption that all the wind energy input is used for the wave growth and that during the wave growth the wave frequency remains constant. In the development of the wind-generated waves, the energy near the dominant wave frequency is continuously redistributed into lower and higher frequency ranges as the consequences of Benjamin-Feir (1967) instability and/or Hasselmann's nonlinear wave-wave interaction (if the fetch is very large). The energy to the lower frequency range will lead to the down shifting of dominant wave frequency and the energy to the higher frequency range is either dissipated for the generation of current or for the maintenance of the saturation range spectrum. This frequency down shifting and higher frequency range dissipation may consume considerable amounts of the wind energy input and the observed $\partial\hat{E}/\partial\hat{x}$ may consequently be lower than that estimated by (7.9).

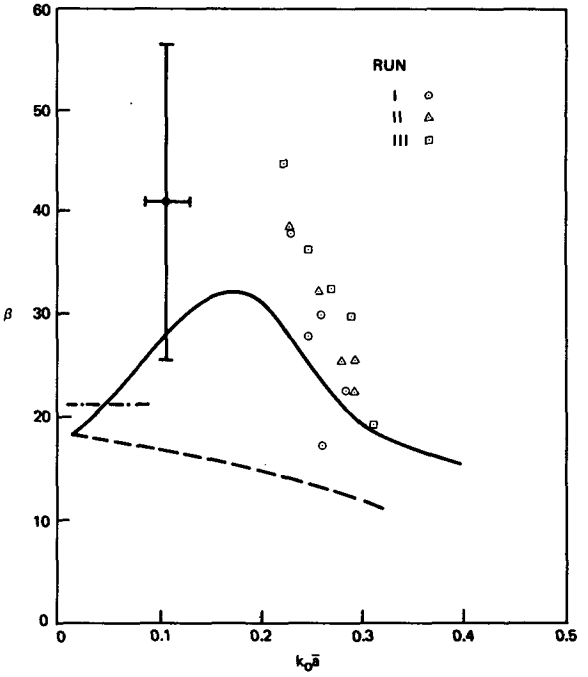

FIG. 9. Wave-induced pressure form drag coefficient β as a function of the wave slope $k_0\bar{a}$. The predictions are from Miles (1960), dot-dashed; Gent (1977), dashed; and Al-Zanaidi and Hui (1981), solid. The dots, in addition to those from Runs I, II, III, are shown by the capped lines from Snyder *et al.* (1981).

8. Concluding remarks

The expressions for momentum and energy transfer across the interface of an air-water coupling system were derived generally for two-dimensional wind waves. The results indicated that a precise estimate of the momentum and energy budgets between the wind and the waves requires measurement of the two-dimensional wave field, all three air velocity components, and the air pressure in a wave-following sense. However, a simple laboratory experiment which consisted of a point measurement of the wind waves, a two-component measurement of the velocity in the mean wind and vertical directions, and a measurement of air pressure in a fixed frame provided us an estimate of the momentum and energy budgets, because the wind waves in a laboratory are presumed to be forced bound waves with a narrow directional spreading function. Hence, our earlier wind wave data obtained by Wu *et al.* (1977) were used in this study to estimate the budgets. However, the results given in Tables 2 and 3 are subject to approximately 20% uncertainty as a result of the fixed frame measurement and of the estimate of $\bar{u}_0$.

Based on the laboratory results of this study, we conclude 1) that the mean wind is typically a turbulent boundary layer flow, having a log-linear velocity profile and a wake characteristic near the free stream; 2) that the wind-generated waves are predominantly forced, bound, nonlinear waves since $k_0\bar{a}$ is large; 3) that the wave-induced air flow is mainly produced by the forced bound wave motion of the surface waves; 4) that the wind momentum and energy are transferred to waves primarily in the frequency range near that of the dominant wave; 5) that the momentum and energy transfer to waves is dominated by the wave-induced pressure; and 6) that the wind waves receive only about 29% of the total energy transfer across the interface while they support approximately 61% of the total momentum transferred from the wind.

The low percentage of total energy received by the waves is a consequence of the high $\bar{u}_0/c_0$ in a laboratory tank. If to the first approximation the turbulent transfer and the effect of wave directional spreading are neglected, the energy transfer to waves is expressed as $\bar{E}_w = \bar{M}_{w1}(c_0 - \bar{u}_0)$. With $\bar{E}_c = \bar{M}_1\bar{u}_0$, the relation between γ_E and γ_M is given by

$$\gamma_M = \frac{\gamma_M(1 - \alpha_0)}{\alpha_0 + \gamma_M(1 - \alpha_0)}, \tag{8.1}$$

where $\alpha_0 = \bar{u}_0/c_0$. In (8.1), α_0 and $\gamma_M(1 - \alpha_0)$ represent the energy transfers to current and waves, respectively, as normalized by $\bar{M}_1c_0$. When $\alpha_0 = 0$, we have

$\gamma_E = 1$, i.e., all the energy transferred across the interface is received by the waves; γ_E is less dependent on γ_M when α_0 is small. The experiment performed by Hsu *et al.* (1981, 1982) belongs to the case of small α_0 and they found γ_E to be about 0.95. When α_0 increases from zero, the leakage of the energy received by the waves to the current increases. The energy $\bar{E}_c$, received by the current, actually consists of the energy leakage from the waves, $\bar{M}_{w1}\bar{u}_0$, and the energy transferred by the mean turbulent shear stress, $\bar{M}_{c1}\bar{u}_0$. These lead to the considerably lower γ_E as observed in this experiment.

The dependence of $k_0\bar{a}$ on the fetch suggests that the sea state evolves from a strong nonlinear wind wave system at short fetch to an almost linear-free wave system at very long fetch. The degree to which the wind wave system behaves as a nonlinear bound wave system or as a linear free wave system depends on whether the components in the frequency range $f > 1.5\, f_0$ are contributed from the nonlinear forced harmonic motion of the dominant wave undergoing self-induced modulations under the influence of the wind or from the free short waves generated by the wind or by wave-breaking. At short fetch, $k_0\bar{a}$ is high and the forced harmonic motion is strong; the free short waves are more likely to be generated locally by wind and wave-breaking; short waves are unlikely to survive over one period of the dominant wave which tends to cause the free short waves to break. As a result of the dominance of the forced harmonic motion, the wave system at short fetch is nonlinear. As $k_0\bar{a}$ decreases and the dominant wavelength increases with increasing fetch (see also Fig. 5), the nonlinear forced harmonic components decrease in magnitude and the wind-generated short waves are more likely to survive the influence of dominant wave. The wind wave system then evolves gradually into a linear free wave system at large fetch. It is expected that at large fetch the nonlinear wave-wave interaction mechanism of Hasselmann (1962, 1963, 1966, 1967) may assume its role in describing the evolution of the wave field. The field measurements of wind waves were in the range of $10^5 < \hat{x} < 10^8$ and $k_0\bar{a} \approx 0.1$; it seems that both the wave-wave interaction of Hasselmann and the nonlinear wave modulation and recurrence mechanism of Lake and Yuen may have a significant role in describing such wind wave systems. At short fetch, the short waves riding on the dominant wave may be significant only in determining the surface roughness which may alter the wind turbulence structure in relation to the momentum and energy transfer to the dominant wave; at large fetch, the short waves may also receive considerable amounts of energy from the wind and then redistribute it to the dominant wave through nonlinear wave-wave interaction.

To obtain insights to the evolution of the wave linearity, we reexamine Fig. 4. While the linear relation $\hat{E} = 1.6 \times 10^{-4}\hat{x}$ is more acceptable, the dependence of $\hat{f}_0$ on $\hat{x}$ is still controversial. There are several mechanisms that can lead to the down-shifting of the dominant-wave frequency. Phillips (1977, p. 168) showed that a mechanism based on Hasselmann's nonlinear wave-wave interaction theory will result in $\hat{f}_0 \propto \hat{x}^{-1/2}$; this is quite inconsistent with the results of Fig. 4. Phillips (1977) then attributed the down-shifting of the dominant-wave frequency as the result of the successive transition of the steep forward face of the wave spectrum to an exponential growth under the action of the wind. Consequently, he found that f_0 is given by (7.5) if $\zeta = 0.05(u_*/c_0)^2$. Apparently, this second mechanism based on the transition of the exponential growth agrees very well with the field data in the range of $10^5 < \hat{x} < 10^7$ since it also predicts a constant value of $\beta = 41$ which appears to be consistent with the field data. As mentioned earlier (Fig. 5), this would also imply that $k_0\bar{a}$ is independent of $\bar{x}$ and is equal to 0.087.

At short fetch, the value of $k_0\bar{a}$ is considerably larger than 0.087 and is dependent on $\bar{x}$; hence, the mechanism based on the transition of the exponential growth due to wind action is probably influential but is not the dominant mechanism for the frequency down-shifting. Since $k_0\bar{a}$ is large the wind-generated waves at short fetch are highly nonlinear. Nonlinear wave is unstable to side-band frequency perturbation and exhibits the recurrence of self-modulation and de-modulation (Yuen and Lake, 1980). From the dimensional argument, the rate of the down-shifting is expected to be characterized by the most unstable side band which is located at frequencies different from the dominant-wave frequency by $k_0\bar{a}f_0$ and has a growth rate equal to $\pi(k_0\bar{a})^2 f_0$. Hence, the nondimensional form for the down-shifting is expressed as

$$\frac{d\hat{f}_0}{d\hat{x}} = -A(2\pi)^2(k_0\bar{a})^3\hat{f}_0^3, \tag{8.2}$$

where A is a proportional constant. From the dispersion relation, we also have

$$\hat{E} = \tfrac{1}{2}(k_0\bar{a})^2(2\pi\hat{f}_0)^{-4}. \tag{8.3}$$

Assuming that the dependence of $\hat{E}$ on $\hat{x}$ is given by (7.3) and solving for $\hat{f}_0$ and $k_0\bar{a}$ from (8.2) and (8.3), we find

$$\hat{f}_0 = 0.35\mathrm{A}^{-1/8}\hat{x}^{-5/16}, \tag{8.4}$$

$$k_0\bar{a} = 0.086\mathrm{A}^{-1/4}\hat{x}^{-1/8} = 0.063\mathrm{A}^{-1/5}(c_0/u_*)^{-2/5}. \tag{8.5}$$

For comparisons, the predictions based on (8.4) and (8.5) with $A = 4.8 \times 10^{-4}$ are also shown in Figs. 4 and 5, respectively. Apparently, the mechanism based on the nonlinear wave evolution to the first approximation describes reasonably well the frequency down-shifting as well as the decrease in the wave non-

linearity. The slightly higher down-shifting rate as observed at short fetch may be due to the influence of the wind action; the wind tends to enhance the growth rate of the side band. At large fetch when $k_0\bar{a}$ becomes small, the transition of the exponential growth due to wind action may eventually take the role of Benjamin-Feir instability in manifesting the down-shifting of the dominant-wave frequency. A stochastic modeling of wind action for wind-wave evolution was provided by Toba (1978).

The evolution from nonlinear wind waves at short fetch to linear wind waves at large fetch is also evident from the measured saturation range constant β_s (Phillips, 1958). The observations in laboratory (Mitsuyasu and Rikiishi, 1978) and in the ocean (Hasselmann *et al.*, 1973, 1976; Mitsuyasu, 1977) show that the wind wave spectrum in the gravity wave range (near the dominant wave frequency) has a similar form given by

$$E(f) = 2S_{\tilde{\eta}}(f) = \beta_s g^2(2\pi)^{-4} f^{-5}\phi(f/f_0), \quad (8.6)$$

where ϕ is the shape function. The integration of (8.6) with respect to f from 0 to ∞ leads to

$$\hat{E} = C_s\beta_s(2\pi\hat{f}_0)^{-4}, \quad (8.7)$$

where

$$C_s = \int_0^\infty y^{-5}\phi(y)dy.$$

It is noted that C_s may take different values in the laboratory and ocean since the shape functions are different; we find $C_s = 0.25$ from field data of Hasselmann *et al.* (1976), while $C_s = 0.50$ from the data of Mitsuyasu and Rikiishi (1978). The comparison of (8.3) with (8.7) provides

$$\beta_s = (k_0\bar{a})^2/2C_s\,. \quad (8.8)$$

Hence, from (8.4) and (8.5) with $A = 4.8 \times 10^{-4}$ we find

$$\beta_s = \frac{0.17}{C_s}\,\hat{x}^{-1/4}. \quad (8.9)$$

As viewed from (8.8), the existence of a similar wave spectrum in gravity-wave range would imply the energy level in the saturation range (which is proportional to β_s) is mainly contributed from the forced harmonic motion of the dominant wave, since the energy density of the forced harmonic motion increases to the first approximation with $(k_0\bar{a})^2$.

A comparison of β_s obtained by this experiment with those compiled by Hasselmann *et al.* (1973) for wave-tank and field measurements is given in Fig. 10. More details for the ocean data shown in Fig. 10 can also be found in Phillips (1977, Fig. 4.9). The dashed-line curve is the empirically-fitted result by Hasselmann *et al.* (1973) and the solid-line curves are the predictions of (8.9) with $C_s = 0.25$ and 0.5. The value of $\beta_s = 0.0081$ for a fully developed spectrum of the form proposed by Pierson and Moskowitz (1964) is also shown in Fig. 10.

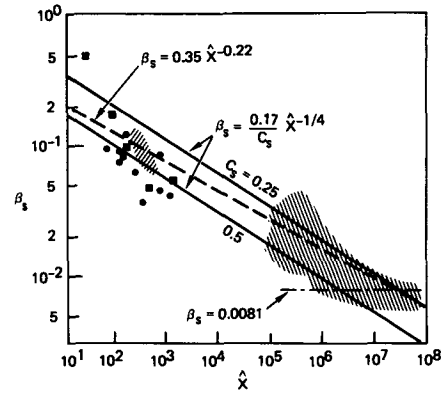

FIG. 10. The dependence of saturation range constant β_s on the nondimensional fetch $\hat{x}$. Hatching (NW–SE), ocean data (see Phillips, 1977, p. 148); (●) (Mitsuyasu, 1968) and (■) (Sutherland, 1968), laboratory data; and hatching (SW–NE), this study.

In this study, the wind energy input to the waves is presumed to be a local process as primarily described by Deardorff's (1967) model of form drag over the dominant wave, except that $k_0\bar{a}$ is not presumed to be constant. The evaluation of the drag coefficient

$$\beta = 2\overline{\tilde{p}(\partial\tilde{\eta}/\partial x_1)}/\rho u_*^2(k_0\bar{a})^2$$

based on our experimental results showed that the dependence of β on x_1 may be the consequence of the dependence of β on the wave slope $k_0\bar{a}$ because $k_0\bar{a}$ is indirectly a function of x_1. The discrepancy among the measurements by Dobson (1971), Elliott (1972) and Snyder (1974) was not resolved by the present experiment. From the recent laboratory results of Hsu *et al.* (1982) and field results of Snyder *et al.* (1981), the high values of β observed by Dobson (1971) may be due to the presence of significant currents running against the wind. Currents against the wind may so strongly reduce the generation of short waves by wind action, wave breaking and nonlinear wave-wave interaction that the surface condition in Dobson's experiment might be aerodynamically smooth. Hsu *et al.* (1982) observed that $\beta = 140$ for wind over a smooth mechanically-generated water wave at $c/u_* = 18.2$.

Acknowledgment. H. Y. Wu was supported by National Science Foundation Grant ENG-73-04190 and Office of Naval Research Contract N00014-76-C-0155, while he was at the Department of Civil Engineering, Stanford University. This work was supported by the National Science Foundation through CME-78-17618 (when the first author was at Stanford University) and OCE-81-00517, and by the TRW IR&D Ocean Surface Physics Project.

REFERENCES

Al-Zanaidi, M. A., and W. H. Hui, 1981: A numerical turbulence model for air flow over water waves. Paper presented at IUCRM Symposium on Wave Dynamics and Radio Probing of the Ocean Surface, Miami Beach.

Barnett, T. P., 1968: On the generation, dissipation, and prediction of wind-waves. *J. Geophys. Res.*, **73**, 513–529.

——, and A. J. Sutherland, 1968: A note on an overshoot effect in wind-generated waves. *J. Geophys. Res.*, **73**, 6879–6885.

——, and J. C. Wilkerson, 1967: On the generation of ocean wind waves as inferred from airborne radar measurements of fetch-limited spectra. *J. Mar. Res.*, **25**, 292–321.

Benilov, A. Y., O. A. Kouznetsov and G. N. Panin, 1974: On the analysis of wind wave-induced disturbances in the atmospheric turbulent surface layer. *Bound.-Layer Meteor.*, **6**, 269–285.

Benjamin, T. B., and J. E. Feir, 1967: The disintegration of wave trains on deep water. *J. Fluid Mech.*, **27**, 417–430.

Benney, D. J., and R. F. Bergeron, 1969: A new class of nonlinear waves in parallel flows. *Stud. Appl. Math.*, **48**, 181–204.

Bole, J. B., and E. Y. Hsu, 1969: Response of gravity water waves to wind excitation. *J. Fluid Mech.*, **35**, 657–675.

Charnock, H., 1955: Wind stress on a water surface. *Quart. J. Roy. Meteor. Soc.*, **81**, 639–640.

Davis, R. E., 1970: On the turbulent flow over a wavy boundary. *J. Fluid. Mech.*, **42**, 721–731.

——, 1972: On prediction of the turbulent flow over a wavy boundary. *J. Fluid Mech.*, **52**, 287–306.

Deardorff, J. W., 1967: Aerodynamic theory of wave growth with constant wave steepness. *J. Oceanogr. Soc. Japan*, **23**, 278–297.

Dobson, F. W., 1971: Measurements of atmospheric pressure on wind-generated sea waves. *J. Fluid Mech.*, **48**, 91–127.

——, and J. A. Elliott, 1978: Wave-pressure correlation measurements over growing sea waves with a wave follower and fixed height pressure sensors. *Turbulent Fluxes Through the Sea Surface, Wave Dynamics and Prediction*, Plenum, 421–432.

Elliott, J. A., 1972: Microscale pressure fluctuations near waves being generated by the wind. *J. Fluid Mech.*, **54**, 427–448.

Gent, P. R., 1977: A numerical model of the air flow above water waves. Part 2. *J. Fluid Mech.*, **82**, 349–369.

——, and P. A. Taylor, 1976: A numerical model for the air flow above water waves. *J. Fluid Mech.*, **77**, 105–128.

Hasselmann, K., 1962: On the nonlinear energy transfer in a gravity wave spectrum. Part 1. *J. Fluid Mech.*, **12**, 481–500.

——, 1963: On the nonlinear energy transfer in a gravity wave spectrum. Part 2. *J. Fluid Mech.*, **15**, 273–281. Part 3, *Ibid.*, **15**, 385–398.

——, 1966: Feynman diagrams and interaction rules for wave-wave scattering. *Rev. Geophys.*, **4**, 1–32.

——, 1967: Nonlinear interactions treated by the methods of theoretical physics (with application to the generations of waves by wind). *Proc. Roy. Soc. London*, **A299**, 77–100.

——, *et al.*, 1973: Measurements of wind wave growth and swell decay during the Joint North Sea Wave Project (JONSWAP). *Heraus. Dtsch. Hydrograph. Inst.*, Reihe A, No. 12, 95 pp.

——, D. G. Ross, P. Müller and W. Sell, 1976: A parametric wave prediction model. *J. Phys. Oceanogr.*, **6**, 200–228.

Hidy, G. M., and E. J. Plate, 1966: Wind action on water standing in a laboratory channel. *J. Fluid Mech.*, **26**, 651–687.

Hsu, E. Y., 1965: A wind water-wave research facility. Dept. Civil Eng. Tech. Rep. No. 57, Stanford University.

Hsu, C. T., E. Y. Hsu and R. L. Street, 1981: On the structure of turbulent flow over a progressive water wave: theory and experiment in a transformed wave-following coordinate system. *J. Fluid Mech.*, **105**, 81–117.

——, —— and ——, 1982: On the transfer of wind momentum and energy across an interface with a progressive water wave. *J. Fluid Mech.* (in press).

——, and ——, 1982: On the structure of turbulent flow over a progressive water wave: theory and experiment in a transformed wave-following coordinate system, Part 2. *J. Fluid Mech.* (in press).

Kawai, S., 1979: Generation of initial wavelets by instability of a coupled shear flow and their evolution to wind waves. *J. Fluid Mech.*, **93**, 661–703.

Keulegan, J. H., 1951: Wind tides in small closed channels. *J. Res. Natl. Bur. Stand.*, **46**, 358–381.

Lake, B. M., and H. C. Yuen, 1978: A new model for nonlinear wind waves. Part 1. Physical model and experimental evidence. *J. Fluid Mech.*, **88**, 33–66.

——, ——, H. Rungaldier and W. E. Ferguson, 1977: Nonlinear deep-water waves: theory and experiment—Part 2. Evolution of a continuous wave train. *J. Fluid Mech.*, **83**, 49–74.

Larson, T. R., and J. W. Wright, 1975: Wind-generated gravity-capillary waves: Laboratory measurements of temporal growth rates using microwave backscatter. *J. Fluid Mech.*, **70**, 417–436.

Long, R. B., 1971: On generation of ocean waves by a turbulent wind. Ph.D. dissertation, University of Miami.

Miles, J. W., 1957: On the generation of surface waves by shear flows. *J. Fluid Mech.*, **3**, 185–204.

——, 1960: On the generation of surface waves by turbulent shear flows. *J. Fluid Mech.*, **7**, 469–478.

——, 1962: On the generation of surface waves by shear flows. Part 4. *J. Fluid Mech.*, **13**, 433–448.

Mitsuyasu, H., 1966: Interactions between water waves and wind (I). *Rep. Res. Inst. Appl. Mech., Kyushu Univ.*, **14**, 67–88.

——, 1968: On the growth of the spectrum of wind-generated waves. 1. *Rep. Res. Inst. Appl. Mech., Kyushu Univ.*, **16**, 459–482.

——, 1977: Measurement of the high-frequency spectrum of ocean surface waves. *J. Phys. Oceanogr.*, **7**, 882–891.

——, and K. Rikiishi, 1978: The growth of duration limited wind waves. *J. Fluid Mech.*, **85**, 705–730.

——, F. Tasai, T. Shuhara, S. Mizuno, M. Ohkusu, T. Honda and K. Rikiishi, 1975: Observations of the directional spectrum of ocean waves using a cloverleaf buoy. *J. Phys. Oceanogr.*, **5**, 750–760.

Müller, P., 1976: Parameterization of one-dimensional wind wave spectra and their dependence on the state of development. *Hamburger Geophys. Einzelschr.*, No. 31, G.M.L. Wittenborn Sohne, Hamburg.

Phillips, O. M., 1957: On the generation of waves by turbulent wind. *J. Fluid Mech.*, **2**, 417–445.

——, 1958: The equilibrium range in the spectrum of wind-generated waves. *J. Fluid Mech.*, **4**, 426–434.

——, 1977: *The Dynamics of the Upper Ocean*, 2nd ed. Cambridge University Press, 336 pp.

——, and M. L. Banner, 1974: Wave breaking in the presence of wind drift and swell. *J. Fluid Mech.*, **66**, 625–640.

Pierson, W. J., and L. Moskowitz, 1964: A proposed spectrum form for fully developed wind seas based on the similarity theory of S. A. Kitaigorodskii. *J. Geophys. Res.*, **69**, 5181–5190.

Plant, W. J., 1982: A relationship between wind stress and wave slope. *J. Geophys. Res.*, **87**, 1961–1967.

Ramamonjiarisoa, A., and J. Coantic, 1976: Loi experimentale de dispersion des vagues produites par le vent sur une faible longueru d'action. *C. R., Acad. Sci. Paris*, **282**.

Rikiishi, K., 1978: A new method for measuring the directional wave spectrum. Part I. Description. *J. Phys. Oceanogr.*, **8**, 508–517. Part II. Measurement of the directional spectrum and phase velocity of laboratory wind waves. *Ibid.*, **8**, 518–529.

Robinson, J. L., 1974: The inviscid nonlinear instability of parallel shear flows. *J. Fluid Mech.*, **63**, 723–752.

Saeger, J. C., and W. C. Reynolds, 1971: Perturbation pressures over travelling sinusoidal waves with fully developed turbulent shear flow. Dept. Mech. Eng. Tech. Rep. No. FM-9, Stanford University, 155 pp.

Schlichting, H., 1968: *Boundary Layer Theory.* McGraw-Hill.

Shemdin, O. H., and E. Y. Hsu, 1967: Direct measurement of aerodynamic pressure above a simple progressive gravity wave. *J. Fluid Mech.,* **30,** 403–416.

Snyder, R. L., 1974: A field study of wave-induced pressure fluctuations above surface gravity waves. *J. Mar. Res.,* **32,** 497–531.

——, and C. S. Cox, 1966: A field study of the wind generation of ocean waves. *J. Mar. Res.,* **24,** 141–178.

——, F. W. Dobson, J. A. Elliott and R. B. Long, 1981: Array measurement of atmospheric pressure fluctuations above surface gravity waves. *J. Fluid Mech.,* **102,** 1–59.

Sutherland, A. J., 1968: Growth of spectral components in a wind-generated wave train. *J. Fluid Mech.,* **33,** 545.

Takeuchi, K., and T. R. Mogel, 1975: A performance evaluation of a minicomputer. *Rev. Sci. Instrum.,* **46,** 686–691.

Toba, Y., 1978: Stochastic form of the growth of wind waves in a single-parameter representation with physical implications. *J. Phys. Oceanogr.,* **8,** 494–507.

Townsend, A. A., 1972: Flow in a deep turbulent boundary layer over a surface distorted by water waves. *J. Fluid Mech.,* **55,** 719–753.

Valenzuela, G. R., 1976: The growth of gravity-capillary waves in a coupled shear flow. *J. Fluid Mech.,* **76,** 229–250.

Wiegel, R. L., 1964: *Oceanographical Engineering.* Prentice-Hall.

Wu, J., 1968: Laboratory studies of wind-wave interactions. *J. Fluid Mech.,* **34,** 91–111.

——, 1972: Physical and dynamical scales for generation of wind waves. *Proc. ASCE,* **98 WW2,** 163–175.

——, 1975: Wind-induced drift currents. *J. Fluid Mech.,* **68,** 49–70.

——, E. Y. Hsu and R. L. Street, 1977: The energy transfer due to air-input, nonlinear wave-wave interaction and white-cap dissipation associated with wind-generated waves. Dept. Civil Eng. Tech. Rep. No. 207, Stanford University, 158 pp.

——, —— and ——, 1979: Experimental study of nonlinear wave-wave interaction and white-cap dissipation of wind-generated waves. *Dyn. Atmos. Oceans,* **3,** 55–78.

Yu, H. Y., E. Y. Hsu and R. L. Street, 1973: Wave-induced perturbation in a turbulent boundary layer over progressive water waves. Dept. Civil Eng. Tech. Rep. No. 172, Stanford University, 135 pp.

Yuen, H. C., and B. M. Lake, 1979: A new model for nonlinear wind waves. Part 2. Theoretical model. *Stud. Appl. Math.,* **60,** 261–270.

——, and ——, 1980: Instabilities of waves on deep water. *Annual Review of Fluid Mechanics,* Vol. 12, Annual Reviews, 303–334.